Pulmonary mesenchymal stem cells are engaged in distinct steps of host response to respiratory syncytial virus infection

Melanie Brügger[1,2,3], Thomas Démoulins[1,2,§], G. Tuba Barut[1,2,3,§], Beatrice Zumkehr[1,2], Blandina I. Oliveira Esteves[1,2], Kemal Mehinagic[1,2,3], Quentin Haas[4], Aline Schögler[5], Marie-Anne Rameix-Welti[6], Jean-François Eléouët[7], Ueli Moehrlen[8], Thomas M. Marti[5,9], Ralph A. Schmid[5,9], Artur Summerfield[1,2], Horst Posthaus[2,10], Nicolas Ruggli[1,2], Sean R. R. Hall[5,9,11], and Marco P. Alves[1,2,#]

[1]Institute of Virology and Immunology, Bern, Switzerland

[2]Department of Infectious Diseases and Pathobiology, Vetsuisse Faculty, University of Bern, Bern, Switzerland

[3]Graduate School for Cellular and Biomedical Sciences, University of Bern, Bern, Switzerland

[4]Institute of Pharmacology, University of Bern, Bern, Switzerland

[5]Department of Biomedical Research, University of Bern, Bern, Switzerland

[6]Université Paris-Saclay, INSERM, Université de Versailles St. Quentin, UMR 1173 (2I), Versailles, France

[7]Université Paris-Saclay, INRAE, UVSQ, VIM, Jouy-en-Josas, France

[8]Pediatric Surgery, University Children's Hospital Zurich, Zurich, Switzerland

[9]Department of General Thoracic Surgery, Inselspital, Bern University Hospital, University of Bern, Switzerland

[10]Institute of Animal Pathology, Vetsuisse Faculty, University of Bern, Bern, Switzerland

[11]Gillies McIndoe Research Institute, Wellington, New Zealand

[§]These authors contributed equally to this work

[#]Corresponding author: marco.alves@vetsuisse.unibe.ch

Word count abstract: 154

Word count manuscript: 7413

References: 75

Figures: 6

Supporting information: 6 figures, 4 tables

ABSTRACT

Lung-resident (LR) mesenchymal stem and stromal cells (MSCs) are key elements of the alveolar niche and fundamental regulators of homeostasis and regeneration. We interrogated their function during virus-induced lung injury using the highly prevalent respiratory syncytial virus (RSV) which causes severe outcomes in infants. We applied complementary approaches with primary pediatric LR-MSCs and a state-of-the-art model of human RSV infection in lamb. Remarkably, RSV-infection of pediatric LR-MSCs led to a robust activation, characterized by a strong antiviral and pro-inflammatory phenotype combined with mediators related to T cell function. In line with this, following *in vivo* infection, RSV invades and activates LR-MSCs, resulting in the expansion of the pulmonary MSC pool. Moreover, the global transcriptional response of LR-MSCs appears to follow RSV disease, switching from an early antiviral signature to repair mechanisms including differentiation, tissue remodeling, and angiogenesis. These findings demonstrate the involvement of LR-MSCs during virus-mediated acute lung injury and may have therapeutic implications.

Keywords: mesenchymal stem and stromal cells, respiratory syncytial virus, acute lung injury, repair and regeneration, bronchiolitis, interstitial pneumonia, respiratory virus infection.

AUTHOR SUMMARY

27 This work identifies a novel function of lung-resident MSCs during virus-induced acute lung injury.
28 These findings contribute to the understanding of host response and lung repair mechanisms
29 during a highly prevalent clinical situation and may have therapeutic implications.

30

31 **INTRODUCTION**

32 The ability of organs to maintain homeostasis and regenerate following injury is vital to an
33 organism. These processes are maintained by many supportive cells including tissue-resident
34 mesenchymal stem and stromal cells (MSCs). MSCs are found in nearly every vascularized tissue
35 including the respiratory tract. More specifically, they are localized in perivascular niches of small
36 and larger blood vessels and were shown to be lung-resident [1-3]. Lung-resident (LR)-MSCs can
37 promote alveolar cell growth, differentiation, and self-renewal. This is of particular importance for
38 epithelial maintenance as well as for repair and regeneration as demonstrated in artificial rodent
39 models of lung injury [4-6]. Failure of these mechanisms may play a role in the etiology of several
40 chronic lung diseases [7, 8]. LR-MSCs can directly interact with various pulmonary immune cell
41 populations via cellular contact or in a paracrine manner by secretion of soluble factors [9].
42 Characterization of immunomodulatory properties of mesenchymal cells are of great clinical
43 importance since non-resident MSCs are the subject of cell-based treatment approaches for
44 various lung disorders [10, 11].

45 In the alveolar niche, LR-MSCs can interact with epithelial cells (AECs), which are the primary
46 cellular target of most respiratory viruses [12-14]. Among them, the human respiratory syncytial
47 virus (RSV) is of high prevalence and causes a huge burden on public health systems. Globally,
48 RSV is the leading cause of severe acute lower respiratory tract infections in early childhood and
49 suspected to have an underestimated impact on the elderly [15, 16]. Several animal models have
50 been established to study RSV infection, with the lamb model best reflecting anatomical and
51 immunological properties of the neonatal human lung. This model recapitulates the clinical
52 features of the human pediatric disease and the closely related bovine RSV is a natural pathogen
53 of ruminants. Furthermore, unlike rodents, lambs present a similar lung development, are
54 susceptible to human RSV, and develop comparable pulmonary lesions [17-19].

55 Despite intense research on MSCs, no information is available about their role during acute
56 respiratory infection and their contribution following virus-induced injury. Given the important role
57 of the mesenchymal compartment and LR-MSCs in lung regeneration and repair, we hypothesize
58 that this applies during respiratory virus infection. Therefore, we aimed to explore the role of the

59 pulmonary mesenchymal compartment, in particular LR-MSCs, during RSV infection using an
60 experimental approach based on primary LR-MSCs isolated from human pediatric donors and a
61 translational model of human RSV infection in lamb.
62

63 ## RESULTS

64 ### LR-MSCs are highly permissive to RSV infection

65 To study the immunobiology of LR-MSCs during respiratory virus infection, we determined first if
66 these cells are susceptible towards RSV infection in comparison to a well described cellular target
67 of RSV, namely AECs. We characterized the LR-MSCs isolated from pediatric donors according
68 to the three criteria proposed by the Mesenchymal and Tissue Stem Cell Committee of the
69 International Society for Cellular Therapy [20]. As shown in **Fig. 1A,** LR-MSCs were positive for
70 the three MSC surface markers CD73, CD90, and CD105. Additionally, we confirmed plastic
71 adherence of the cells and their trilineage potential by differentiating them towards chondrocytes,
72 osteocytes, and adipocytes (**Fig. 1B**). Next, we assessed mRNA expression levels of different
73 putative RSV cell-surface receptors/co-receptors [21-24], namely nucleolin, toll-like receptor 4
74 (TLR4), intercellular adhesion molecule 1 (ICAM-1), and annexin II in pediatric LR-MSCs in
75 comparison to donor-matched AECs. All tested receptors were expressed in both cell types, while
76 mRNA levels were significantly higher in LR-MSCs in comparison to AECs for all the receptors
77 tested (**Fig. 1C**), suggesting that LR-MSCs are susceptible to RSV infection. Thereby, we
78 detected fast replication kinetics of RSV in LR-MSCs similar to levels measured in infected AECs
79 (**Fig. 1D**). To confirm the susceptibility of LR-MSC to other RSV strains, we infected LR-MSCs
80 with a clinical isolate of RSV subtype A (RSV-ON1-H1). While after 24 to 48 hours post-infection
81 (p.i.) around 80% of LR-MSCs were infected by RSV-A2, the clinical isolate showed slower
82 kinetics of infection by reaching 50% of RSV-positive cells within 48 hours p.i. However, 6 days
83 p.i., both RSV-A2 and RSV-ON1-H1 infected nearly 100% of the cells (**Fig. 1E**). Given that LR-
84 MSCs are highly susceptible to RSV infection, we were wondering how the virus spreads among
85 the cells. To follow visually virus spread in the two different cell types, we used a recombinant
86 RSV expressing constitutively the mCherry reporter. While infected well-differentiated (WD)-

87 AECs appear as discrete RSV-positive cells, infected LR-MSCs showed up in discrete foci,
88 suggesting RSV spread via cell-to-cell contact (**Fig. 1F**). To further confirm the distinct life cycles,
89 we measured infectious virus release over time in LR-MSCs in comparison to WD-AECs by
90 applying a plaque-forming unit (PFU) assay. Remarkably, at most of the time-points tested, there
91 was significantly higher infectious virus release in the apical washings of infected WD-AECs
92 compared to the supernatants of LR-MSC cultures infected with a low (**Fig. 1G**) or a high
93 multiplicity of infection (MOI) (**Fig. 1H**). Moreover, there was almost no infectious RSV detectable
94 in supernatants of infected LR-MSCs with low or high MOIs (**Fig. 1G, H**). Altogether, these results
95 demonstrate that primary pediatric LR-MSCs are highly permissive to RSV infection and that RSV
96 replicates in LR-MSC, although the life cycle of RSV is distinct to AECs.
97
98 **RSV infection is altering the immune properties of LR-MSCs**
99 We therefore aimed to establish if LR-MSCs can mount an antiviral response upon RSV infection.
100 Twenty-four hours p.i., we observed a significant increased expression of interferon stimulated
101 genes (ISGs) commonly induced during RNA virus infections [25]. More specifically, RSV-A2 and
102 RSV-ON1-H1 infection induced a significant upregulation of retinoic acid-inducible gene-I (RIG-
103 I), melanoma differentiation-associated protein 5 (MDA-5), 2',5'-oligoadenylate synthetase 2
104 (2',5'-OAS), interferon (IFN)-induced dynamin-like GTPase (MxA), and virus inhibitory protein,
105 endoplasmic reticulum-associated, IFN-inducible (Viperin) compared to mock control (**Fig. 2A**).
106 Furthermore, the mRNA levels of both IFN-β and IFN-λ1 had a trend towards significantly higher
107 levels upon RSV infection (**Fig. 2B**). We also verified if RSV infection-induced increased mRNA
108 levels of type I and III IFNs resulted in an increased protein release. IFN-β release was
109 significantly stimulated by the two RSV strains over time and was quantified at highly significant
110 levels after 72 hours p.i. (**Fig. 2C**). Furthermore, the protein levels of IFN-λ1/3 were significantly
111 elevated after 24 hours and maintained at high concentrations up to 72 hours p.i. compared to
112 mock control (**Fig. 2D**). Next, we wanted to evaluate whether infection has an impact on the
113 immunomodulatory properties of LR-MSCs. First, we evaluated the cell-surface expression levels
114 of two co-stimulatory molecules, namely programmed death-ligand 1 (PD-L1) and major

115 histocompatibility complex (MHC) class I, described in LR-MSCs to be involved in their
116 immunomodulatory characteristics [26, 27]. LR-MSCs expressed baseline levels of both co-
117 stimulators. Poly(I:C), a ligand mimicking RNA virus infection, induced a significant upregulation
118 of both co-stimulatory molecules in comparison to mock control. In line with this, RSV infection
119 led to the induction of slightly increased levels of PD-L1 and MHC class I expression compared
120 to mock-treated LR-MSCs, with differences not reaching significance, as shown in representative
121 histograms (**Fig. S1A**) and upon quantification (**Fig. S1B**). Next, we evaluated the secretory
122 profiles of LR-MSCs following RSV infection in comparison to the well described AECs, the
123 primary target of RSV infection *in vivo* [12]. Upon infection of WD-AECs with RSV-A2 or RSV-
124 ON1-H1, the basolateral cytokine secretion revealed mainly CXCL10/IP-10 and CXCL8/IL-8
125 release (**Fig. 2E**). Contrary to WD-AECs, RSV infection of LR-MSCs led to a massive secretion
126 of several cytokines. In fact, 24 and 72 hours p.i., expression was remarkably increased for most
127 of the cytokines measured, including CXCL10/IP-10, CXCL8/IL-8, IL-6, G-CSF, CCL5/RANTES,
128 IL-9, IFN-γ, IL-5, and L-17 to name the most notable ones (**Fig. 2F**). Taken together, these data
129 demonstrate that RSV infection leads to a robust activation of LR-MSCs, characterized by a
130 strong antiviral and pro-inflammatory phenotype combined with cytokines modulating T cell
131 function (**Fig. 2G**).
132
133 **RSV infection is causing lung injury in lamb**
134 To study the MSC compartment of the lung and its role during an acute respiratory virus infection,
135 we applied an *in vivo* approach using the neonatal lamb model of RSV infection. Although data
136 are available on ovine MSCs derived from several tissues, ovine LR-MSCs have not been
137 described yet [28-30]. Thus, we isolated and expanded LR-MSCs cultures from healthy ovine
138 lung cell suspensions as described previously for human tissue [3]. Characterization by
139 immunophenotyping displayed a high level of cell surface markers typically found in MSCs such
140 as the hyaluronate receptor CD44 and CD29 (ITGB1). An additional marker, CD166 (ALCAM),
141 was also expressed on cultured MSCs (**Fig. S2A)**. The plastic-adherent cells were large with a
142 fibroblast-like morphology. Multilineage capacity was confirmed following specific culture

143 conditions, as ovine LR-MSCs transdifferentiated to chondrocytes, osteocytes, and adipocytes
144 (**Fig. S2B**). Before infection of the animals, we performed an infection of ovine LR-MSCs cultures
145 with human RSV. Virus replication was evident as observed by an increase of RSV load of cell-
146 associated viral RNA over time. Furthermore, similarly to RSV-infected human LR-MSCs, the
147 infectious virus in the supernatants was undetectable or close to the detection limit suggesting
148 cell-to-cell spread (**Fig. S2C**). Newborn lambs were infected with human RSV-A2 and respiratory
149 disease was evaluated during the acute (3 and 6 days p.i.), recovery (14 days p.i.), and
150 convalescence (42 days p.i.) phases. To do so, at each timepoint p.i., we examined the lung
151 tissue and the cellular components of bronchoalveolar lavage (BAL) fluid (**Fig. 3A**). RSV-infected
152 neonates showed clear nasal discharge, occasional coughing and wheezing. Macroscopic lesions
153 were detected at necropsies performed 3 and 6 days p.i. Lungs failed to collapse and showed
154 multiple, irregular, mildly reddened areas with slightly increased consistency of up to 2 cm in
155 diameter in all lung lobes. Histopathological evaluation of the lung revealed tissue consolidation,
156 bronchiolitis, and thickening of interalveolar walls 3, and 6 days following RSV infection (**Fig. 3B**).
157 Following infection, AT2 cell hyperplasia was observed, indicating tissue injury (**Fig. S3A**). In
158 addition, at 6 days p.i. few syncytial cells lining alveoli were present (**Fig. S3A, B**). These features
159 disappeared 14 days p.i. (**Fig. 3B**), indicating resolution of lesions after RSV-mediated acute lung
160 injury. We evaluated the viral RNA levels in the lung and BAL tissues. In the lung, the RSV loads
161 decreased over time with no virus detectable in 50% of the animals 14 days p.i. and in all animals
162 42 days p.i. In the cellular fraction of the BAL, RSV copies were highest at 3 days p.i., with viral
163 RNA detectable in 66% of the animals 14 days p.i. and reaching undetectable levels 42 days p.i.
164 There was a significant difference in viral loads with approximately 100 times higher level of RSV
165 copies detectable in the BAL compartment compared to the lung at both, 3 and 6 days p.i. (**Fig.**
166 **3C**). To confirm the histopathological evaluation revealing RSV-mediated tissue injury, we
167 assessed cell death by quantifying cleaved caspase-3-positive cells using an approach
168 summarized in **Fig. S4**. The percentage of cleaved caspase-3 positive cells in the lung, was
169 significantly increased for infected animals 3, and 6 days p.i. and similar 14, and 42 days p.i.
170 compared to mock controls (**Fig. 3D**). Lung injury is further indicated by shedding of apoptotic

171 cells into the bronchoalveolar space. Indeed, there are significantly more cleaved caspase-3
172 positive cells 3 days p.i. assessed for infected compared to mock-infected animals (**Fig. 3E**). The
173 impact of RSV infection on the bronchoalveolar space is further indicated by an infiltration of cells
174 as assessed in the BALs from infected compared to mock-infected animals 3 to 14 days p.i. (**Fig.**
175 **3F**). In summary, the life cycle of RSV is similar in human and ovine LR-MSCs and infection of
176 neonatal lambs with human RSV is causing lung injury. These data support the use of the lamb
177 model to investigate LR-MSCs in RSV disease.
178
179 **LR-MSCs are a target for RSV infection *in vivo***
180 To determine if LR-MSCs can be a target for RSV *in vivo*, we designed an assay allowing the
181 identification of the pulmonary epithelial ($CD31^-CD45^-panCTK^+$) and mesenchymal ($CD31^-CD45^-$
182 $panCTK^-CD29^+CD44^+$) compartments, as well as detection of RSV infection *in vivo* (**Fig. 4A)**. In
183 13-80% of the infected animals, both RSV-positive epithelial cells and LR-MSCs were detected
184 in the lung cell suspensions 3, 6 and 14 days p.i. (**Fig. 4B, S5**). When RSV-positive LR-MSCs
185 were plotted as a function of RSV-positive epithelial cells, a significant positive association was
186 found, suggesting that the spread of RSV infection to LR-MSCs is linked to the extent of
187 replication in the respiratory epithelium (**Fig 4C**). Next, MSCs derived from lung tissue and BALs,
188 were isolated from each animal at the different time points p.i. and expanded in culture. When
189 testing the presence of RSV within the lung-derived MSC cultures, viral RNA was detectable in
190 most cultures from the animals at 3 and 6 days p.i. and in none of the cultures isolated from
191 animals at 14 and 42 days p.i. In line with the higher viral loads in the BAL cellular fraction
192 compared to the lung tissue, we detected high levels of RSV RNA in all BAL-derived MSCs from
193 animals at 3 and 6 days p.i. and from 3 out of 7 animals isolated at 14 days p.i. RSV RNA levels
194 were undetectable in all cultures isolated from animals at 42 days p.i. (**Fig. 4D**). Interestingly, we
195 noticed giant multinucleated cells in cultures derived from infected animals which were never seen
196 for mock animal-derived cultures (**Fig. 4E**). Given that RSV spread in foci and infectious virus
197 was rarely detected in the supernatants of infected human and ovine LR-MSCs cultures, we
198 hypothesized that these phenotypically distinct cells were RSV-infected MSCs. This was

199 confirmed by confocal microscopy visualization (**Fig. 4F**) and by the infection of cultures from
200 human and ovine LR-MSCs with RSV-mCherry (**Fig. S6A, B**). Together, these results indicate
201 that the lung MSC compartment is a target for RSV infection *in vivo* during the early phase of
202 respiratory disease.
203
204 **RSV infection leads to the expansion of the pulmonary MSC niche *in vivo***
205 To investigated the impact of virus-mediate lung injury on LR-MSCs *in vivo*, we analyzed the
206 mesenchymal compartment of RSV-infected newborn lambs during the acute, recovery, and
207 convalescence phases of RSV disease. As a mild to asymptomatic RSV disease control, adult
208 animals were infected for a period of 14 days (**Fig. 5A**). Contrary to RSV-infected neonates,
209 infection of adults did not lead to any notable clinical manifestation nor macroscopic lesions, while
210 rare foci of interstitial thickening with leukocyte infiltrates and mild AT2 hyperplasia were visible
211 histologically (**Fig. 5B**). A colony-forming unit-fibroblast (CFU-F) assay was applied to lung-
212 derived cells from infected and mock-infected animals. This assay is commonly used to assess
213 the proliferative activity of MSCs and their ability to form discrete fibroblast-like colonies [31, 32].
214 The analysis revealed a significant effect of RSV infection on the proliferative properties of LR-
215 MSCs by increasing their activity already 3 days p.i. compared to mock control (**Fig. 5C**).
216 Quantitative analysis confirmed significantly increased CFU-F counts during the acute phase of
217 infection 3 and 6 days p.i. Interestingly, there was still a nonsignificant tendency of more CFU-F
218 counts during later phases of RSV disease 14 and 42 days p.i. compared to age-matched non-
219 infected animals (**Fig. 5D**). CFU-F counts were around 20 times lower for control adults (average
220 CFU-F count of 0.6) in comparison to control neonates (average CFU-F count of 14.2), indicating
221 an age-dependent effect on the steady-state proliferative properties of LR-MSCs. However, RSV
222 infection led to a significant increase of these colonies 14 days p.i. with an average count of 6.3
223 (average CFU-F count of 29.9 for infected neonates 14 days p.i.) (**Fig. 5E, F**). These results
224 provide evidence that RSV infection leads to a stimulation of the proliferative activity and the
225 expansion of the pulmonary MSC pool, particularly in neonates compared to older animals.
226

227 **The transcriptional activity of LR-MSCs is related to the phases of RSV disease**

228 To investigate how RSV infection *in vivo*, we applied an experimental approach developed by
229 Spadafora *et al*., who showed that tracheal aspirate-derived MSCs retain their transcriptional
230 signature following a short expansion in culture [33]. We undertook whole transcriptome analysis
231 from expanded LR-MSCs isolated from infected neonates during the acute, recovery and
232 convalescent phases of RSV disease in comparison to mock-infected neonates. To confirm
233 identity of MSCs expanded in culture, we calculated the transcripts per million (TPM) of markers
234 used for their identification [20, 34]. LR-MSCs had high transcriptional levels of ENG (CD105),
235 NT5E (CD73), THY1 (CD90), ITGB1 (CD29), CD44 and PDGFRA among others, and lacked
236 transcripts of HLA-DR or HLA-DQ, PTPRC (CD45), CD34, ITGAM (CD11b), or PECAM (CD31)
237 confirming their MSC identity (**Fig. 6A**). Next, we compared the transcriptome profiles of LR-
238 MSCs during the acute phase of RSV disease (6 days p.i.) to mock-infected animal-derived LR-
239 MSCs and found 14 differentially expressed genes (DEGs) to be significantly upregulated. The
240 majority of them belong to the IFN pathway and are associated with antiviral responses, such as
241 RSAD2 (Viperin), OASL, ISG15, IFI44, and IFI44L and two pro-apoptotic genes, namely
242 TNFSF10/TRAIL and STC1 (**Fig. 6B**). These findings are in line with our *in vitro* results derived
243 from human LR-MSC and support the idea that LR-MSCs mount an antiviral response against
244 RSV infection *in vivo*. Remarkably, while there was no significant difference in the recovery phase
245 (14 days p.i.) compared to mock-infected control (**Fig. 6C**), there were 43 DEGs differentially
246 expressed in LR-MSCs isolated during the convalescence phase (42 days p.i.) (**Fig. 6D**). Several
247 of these genes are associated with secretory pathway, including MAGE2 (protein trafficking),
248 TBC1D20 (autophagosome maturation), MAP7D3 (microtubule assembly), and MARCHF9
249 (protein processing). In line with this, high transcriptional activity of LR-MSCs during the
250 convalescence phase is evidenced by the upregulation of various non-coding RNAs and
251 ribonuclease proteins involved in pre-RNA processing and regulation of transcription and/or
252 translation. Furthermore, genes linked with differentiation and developmental processes, such as
253 SOX4 NOC3L, and C2CD3 were differentially expressed during the convalescence phase.
254 Remarkably, many of the upregulated DEGs were related to endothelial cell function and

255 angiogenesis, such as TRPC4 or KDR which codes for the vascular endothelial growth factor
256 receptor 2 (VEGFR2), and ITGA9, the receptor of VCAM1. Finally, among the top downregulated
257 DEGs were two genes coding for matrix-metalloproteases (MMPs), MMP1 and MMP3, which are
258 involved in the remodeling of the extracellular matrix (ECM). The list of significant DEGs and
259 associated literature from infected *versus* noninfected animal-derived LR-MSCs is provided in
260 **Table S1.** To confirm the interpretation of our findings, we used a computational method for
261 pathway enrichment analysis of the transcriptional profiles of LR-MSCs over RSV infection. Gene
262 set enrichment analysis (GSEA) revealed that the transcriptional signature of LR-MSCs isolated
263 from RSV- and mock-infected animals is retained during the short culture phase and is following
264 the different phases of respiratory disease. During the acute phase of infection, the significant
265 enriched hallmark gene sets were associated to IFN pathways, inflammation, and stress
266 response. Notably, the only enriched gene set downregulated in the acute phase of RSV infection
267 was Notch signaling, a central pathway regulating cell proliferation and differentiation. During the
268 recovery and the convalescence phases, shared gene sets associated with cell cycle regulation,
269 such as E2F and Myc pathway, were downregulated compared to mock controls. Further, during
270 the convalescence phase of RSV disease, five additional hallmark gene sets were upregulated.
271 More precisely, the transcriptional signature of LR-MSCs isolated from infected animals long after
272 viral clearance revealed processes such as myogenesis, epithelial-mesenchymal transition
273 (EMT), angiogenesis, p53 pathway, and TGF-β signaling, suggesting that LR-MSCs are involved
274 in tissue repair and regeneration following virus-induced injury (**Fig. 6E**). To sum up, these results
275 show that MSCs from the pulmonary alveolar niche, are activated during virus-induced lung injury
276 by an increase in their proliferative activity and by mounting dynamic transcriptional profiles
277 leading to an early antiviral and inflammatory response followed by mechanisms associated with
278 tissue remodeling, repair and regeneration (**Fig. 6F**).
279

280 **DISCUSSION**

281 This work was undertaken to explore the role of the pulmonary MSC compartment during acute
282 respiratory virus infection and its contribution to lung repair. Our investigations herein reveal upon

283 infection, LR-MSCs mount an antiviral response and release a variety of immunomodulatory
284 mediators, which may have a biological impact on the pulmonary microenvironment. Furthermore,
285 we show that RSV-mediated lung injury activates and stimulates the expansion of LR-MSCs
286 which mount a dynamic transcriptional program related to mechanisms of repair and
287 regeneration.
288 Contrary to the well-described replication of RSV in AECs, the primary cellular target of RSV
289 infection, our data indicates a distinct life cycle in LR-MSCs with viral spread via cell-to-cell
290 contact. Such mechanism may improve virus dissemination and promote immune evasion [35].
291 In a humanized mouse model, pulmonary mesenchymal cells were shown to be susceptible to
292 different viruses such as Middle East respiratory syndrome coronavirus, Zika virus, and
293 cytomegalovirus [36]. In addition, they were recently proposed as an immune-privileged niche for
294 *M. tuberculosis* persistence [37]. Since LR-MSCs are described to localize perivascular and in
295 close proximity to AECs, this makes them a potential nonepithelial target for respiratory virus
296 infection. Here, we show accessibility of LR-MSCs possibly through physical disruption of the
297 epithelial barrier. Indeed, already 3 days p.i., we observed evidence of epithelial injury associated
298 with AECs infection and concomitant LR-MSCs targeting by RSV. It is described that RSV
299 infections can lead to a number of extrapulmonary manifestations [38]. Assuming the presence
300 of MSCs in most tissues, it is conceivable that in some predisposed subjects, RSV may target
301 other MSC niches throughout the body. In line with this, bone marrow and umbilical cord vein
302 MSCs were shown to be susceptible to RSV infection *in vitro* [39, 40].
303 We show that RSV infection is signaled by LR-MSCs through the induction of antiviral and pro-
304 inflammatory mediators, both associated with RSV disease severity [41-43]. In addition, RSV
305 infection of LR-MSCs lead to a type I and III IFN release and subsequent ISGs induction, shifting
306 LR-MSCs towards an antiviral state. This is in line with the pro-inflammatory and antiviral
307 transcriptional signatures found in LR-MSCs, isolated form infected animals during the acute
308 phase of RSV disease. In mice, it has been shown that IFN signaling of the lung stromal
309 compartment was protective against influenza virus by reducing viral replication [44]. Massive
310 lung infiltration of immune cells following cytokine release, termed cytokine storm, is characteristic

311 of severe respiratory virus infections including RSV [45]. Among the most abundant chemokines
312 in infants suffering from RSV bronchiolitis are CXCL10/IP-10, CXCL8/IL-8, CCL2/MCP-1 and
313 CCL3/MIP-1α. Similarly, in our setting, RSV infection of LR-MSCs led to a massive release of
314 chemokines with the potential to attract neutrophils, eosinophils, monocytes, and lymphocytes,
315 such as CXCL8/IL-8, CCL5/RANTES, CCL2/MCP-1, and CXCL10/IP-10, respectively. In RSV
316 disease, it is believed that the cellular sources of the pulmonary chemokine responses are AECs
317 and inflammatory immune cells; our data suggests that LR-MSCs might provide an additional
318 source [46].
319 Besides the vast chemokine production, RSV infection of LR-MSCs led as well to the release of
320 a number of other mediators and growth factors. Interestingly, the secretory profile of RSV-
321 infected LR-MSCs was very distinct to the one described for RSV infected BM-MSCs, supporting
322 tissue specificity of MSC populations [39, 47, 48]. Notably, VEGF, a key mediator of angiogenesis,
323 is released by pediatric LR-MSCs at increased levels after RSV infection. Also, the transcriptional
324 profiles of LR-MSCs isolated during the convalescence phase of RSV disease were related to
325 endothelial biology and pathway analysis revealed pro-angiogenic enriched gene sets. In line with
326 this, using an adult rat model, VEGF signaling disruption was shown to cause an enlargement of
327 the air spaces and an alteration of the alveolar structure, suggesting that VEGF has a crucial role
328 during normal adult alveolarization [49]. Considering the perivascular location of MSCs in tissues,
329 our data indicate that LR-MSCs may modulate endothelial cells activity during virus-induced lung
330 injury.
331 TGF-β is a central regulator of the respiratory system and controls epithelial and mesenchymal
332 cell fate through several mechanisms such as promotion of EMT, myofibroblast differentiation,
333 and stimulation of ECM production and remodeling [50]. Our transcriptional data from LR-MSCs
334 isolated from infected animals during the convalescence phase of RSV disease, revealed that
335 these cells might play a role in these mechanisms. Indeed, compared to noninfected control-
336 derived LR-MSCs, their transcriptome profiles are linked with TGF-β signaling and EMT. The later
337 is linked with the acquisition of more proliferative stem-like states providing an additional link
338 between activation of EMT and wound healing [51]. In line with this, the p53 pathway activation

339 further supports the maintenance of MSC stemness for subsequent repair processes [52].
340 Transcriptome analysis of LR-MSCs isolated long after virus clearance, positively associated with
341 myogenesis. Myofibroblasts, an activated type of mesenchymal cells and an important source of
342 ECM, participates in tissue repair but their persistence after wound healing is linked to fibrotic
343 disorders [53]. Thus, failure of these mechanisms may potentially increase the risk of developing
344 fibrotic abnormalities following respiratory virus infections. Comorbidities such as recurrent
345 wheezing and asthma are happening years after RSV infection has resolved. To date, it remains
346 unclear if pulmonary mesenchymal cells deficiency in lung repair and regeneration are linked with
347 such disorders [54, 55].
348 Due to their immunomodulatory properties, MSCs are applied in cell-based therapies with
349 promising outcomes for the treatment of pulmonary morbidities such as idiopathic pulmonary
350 fibrosis (IPF), acute-respiratory distress syndrome (ARDS) and severe influenza infections [10,
351 56-58]. Furthermore, the current coronavirus disease 2019 (COVID-19) pandemic is leading to a
352 strong interest in MSCs as a treatment option for severe COVID-19 cases. As a consequence,
353 an increasing number of clinical investigations of such MSC-based therapy approaches are under
354 evaluation [59-62]. Safety concerns regarding susceptibility of MSCs towards different viruses, as
355 well as potential viral reactivation events have been raised [63]. On one hand, our data indicate
356 eventual safety concerns due to the targeting of LR-MSCs during the acute phase of virus
357 infection. On the other hand, we provide evidence that LR-MSC seem to have a beneficial effect
358 after virus clearance, supporting the use of MSC-based therapies to treat virus-induced lung
359 injury.
360 The ovine lung is a classical model of the human respiratory tract due to similarities in size,
361 structure, development and immune system [64]. However, some limitations should be
362 mentioned. First, we observed a high animal-to-animal variability in most endpoints measured,
363 probably due to the outbred nature of the animals. While this might look like a limitation, we believe
364 it reflects best the situation in humans compared to inbred models. Secondly, we used the isolated
365 LR-MSCs as a single population but previous single-cell transcriptomic studies demonstrated that
366 MSC, are a rather heterogeneous population composed of distinct MSC subsets [4, 5, 65]. Third,

367 due to the lung size, we analyzed three pooled specimens, representative of each lung region.
368 This might explain why we didn't detect RSV-positive cells for some animals for whom productive
369 infection was demonstrated by the assessment of the viral loads.
370 In summary, our data demonstrate the involvement of pulmonary MSCs during respiratory virus
371 infection. While being a target for RSV, these cells can respond to infection by switching to an
372 antiviral state and by a profound remodeling of their immune phenotype. Furthermore, LR-MSCs
373 show hallmarks of tissue repair and regeneration processes after viral clearance. Our findings
374 identify a function of LR-MSCs in a highly prevalent clinical situation and constitute a basis for
375 further exploration of the pulmonary mesenchymal compartment during respiratory viral
376 infections.
377

378 **MATERIAL AND METHODS**

379 **Virus propagation and titration**

380 Human RSV-A2 strain was derived from ATCC (VR-1540, GenBank accession number
381 KT992094.1). The recombinant mCherry-expressing RSV (RSV-mCherry) is described elsewhere
382 and was kindly provided by Prof. Dominique Garcin (University of Geneva, Switzerland)[66]. The
383 clinical RSV isolate, RSV-ON1-H1, was collected from a child below the age of five years with
384 confirmed RSV infection, hospitalized at Hannover Medical School, Germany. The virus was
385 isolated from nasopharyngeal aspirates and was passaged up to five times in HEp-2 cells (ATCC,
386 CCL-23). The caregivers gave informed consent for the donation of nasopharyngeal aspirates,
387 and all steps were conducted in compliance with good clinical and ethical practice and approved
388 by the local ethical committee at Hannover Medical School, Germany (permission number
389 63090/2012) [67]. All RSV strains were propagated on HEp-2 cells, cultivated in DMEM (Gibco)
390 supplemented with 10% fetal bovine serum (FBS, Gibco). Briefly, HEp-2 cells were infected at a
391 MOI of 0.02 PFU/cell for 2 hours before the addition of DMEM supplemented with 5% FBS. The
392 cell-associated virus was harvested by scraping the cell monolayer when 60% of cytopathic effect
393 was observed. The virus was released from the cells by one freeze-thaw cycle followed by
394 centrifugation to get rid of cell debris. Virus stocks were stored in aliquots containing 10% sucrose

395 (Sigma) at -150°C. To prepare a mock control the same procedure was applied without adding
396 virus. For virus titration, serial dilutions of supernatants were added to HEp-2 cells and incubated
397 for 48-96 h at 37°C, 5 % CO_2. Next, the cells were washed with PBS, fixed with methanol
398 supplemented with 2% H_2O_2 and incubated with a biotinylated anti-RSV antibody (Bio-Rad) in
399 PBS containing 1% bovine serum albumin (BSA, Sigma) for 1 h, followed by 30 min incubation
400 with ExtrAvidin Peroxidase (Sigma) and staining with 3,3′-diaminobenzidine substrate (Sigma).
401 Virus titers were expressed as PFU/ml.
402
403 **Primary cells**
404 Primary pediatric MSCs were obtained as described previously [26, 65]. Briefly, healthy lung
405 tissue was obtained from pediatric patients undergoing elective surgery for congenital pulmonary
406 airway malformation and other various airway abnormalities at the Children's University Hospital
407 of Zurich (n=9, age range: 5 days to 181 months, (**Table S2**)). Written informed consent was
408 obtained for all the patients and/or parent/guardian and the study protocol was approved by the
409 local Ethics Commission of the Canton of Bern (KEK-BE:042/2015). Minced tissue was further
410 disaggregated enzymatically using a solution containing collagenase I and II (Worthington
411 Biochemicals) at a concentration of 0.1 and 0.25%, respectively. Further, digestion buffer was
412 supplemented with 0.2 mg/ml deoxyribonuclease I (Biochemicals) to the digestion buffer to
413 prevent cell clumps and improve cell recovery. To isolate MSCs, a flow cytometry (FCM) assay
414 was applied using a panel of fluorescently-conjugated human monoclonal antibodies: CD45,
415 CD14, CD31, and EpCAM for negative and CD73 and CD90 for positive selection. FACS-sorted
416 MSCs were expanded in tissue culture flasks pre-coated with 0.2% gelatin solution (Sigma) and
417 in chemically defined growth medium consisting of α-MEM with ribonucleosides (Sigma)
418 supplemented with 1% FBS, GlutaMAX (Invitrogen), 10 ng/ml of recombinant human fibroblast
419 growth factor 2 (FGF2, Life Technologies), 20 ng/ml of recombinant human epidermal growth
420 factor (EGF, Life Technologies), human insulin (Sigma), 10'000 units/ml of penicillin and 10'000
421 µg/ml streptomycin (Sigma). Cells were maintained in a humidified atmosphere at 37°C, 5% CO_2
422 until confluence was reached. The medium was aspirated carefully and replaced with fresh

423 medium six days after plating and after that point performed twice a week. Cells were used prior
424 to passage 5 in all experiments. WD-AECs isolated from independent healthy donors (MucilAir™,
425 Epithelix Sàrl, Geneva, Switzerland) were used for RSV infection. The cultures were maintained
426 on 24-well transwell inserts (Corning) at the air-liquid interface (ALI) in MucilAir™ culture medium
427 (Epithelix Sàrl, Geneva, Switzerland) in a humidified incubator at 37° C, 5% CO_2. Every 3 days
428 culture medium was changed. The apical surface was rinsed with Hank's balanced salt solution
429 (HBSS, ThermoFisher) once a week and prior to infection, to washout the mucus.
430
431 **RSV infection**
432 To perform infection of primary pediatric LR-MSCs and AECs with RSV-A2, RSV-mCherry, or
433 RSV-ON1-H1, 10^5 cells per well of a 12 well plate were seeded 24 h prior to infection and/or
434 stimulation. Cells were infected at selected MOIs of RSV or mock-control in FBS-free medium for
435 1 h at 37°C and 5% CO_2. Subsequently, cells were washed three times with 1X PBS and then
436 incubated in growth medium. Ten µg/ml of poly(I:C) (Sigma) was applied in growth medium and
437 incubated alike until harvesting. At selected time points, supernatants and cells were harvested
438 and stored appropriately for further analysis. For infection of WD-AECs, virus preparations were
439 diluted in medium and virus dilutions were applied apically to the tissue, assuming an average of
440 500,000 cells per insert. As a mock control, the culture supernatant of mock-infected HEp-2 cells
441 was used. Virus particles were allowed to adsorb for 3 h at 37°C and 5% CO_2 before the inoculum
442 was removed and each insert was carefully washed three times with pre-warmed HBSS and
443 placed on a new well containing fresh MucilAir™ culture medium. For stimulation of the WD-AEC
444 inserts, 10 µg/ml poly(I:C) were applied to the basolateral chamber containing the culture medium.
445 For examination of infectious viral particle release 2, 24, 48, 72, and 144 hours p.i., 250 µl HBSS
446 was added to the apical surface and incubated for 20 min at 37°C, harvested, and stored at −70°C
447 until further analysis. Basolateral media was collected and similarly stored, and replaced with
448 fresh media in the basolateral chamber of the inserts.
449
450 **RNA isolation and quantitative PCR**

451 Total RNA of primary pediatric LR-MSCs, human AECs, and ovine lung- and BAL-derived cultured
452 MSCs was extracted using the Nucleospin® RNA Plus Kit (Macherey-Nagel) according to the
453 manufacturer's protocol. For reverse transcription and synthesis of complementary DNA the
454 Omniscript RT Kit (Qiagen) using random hexamers (Invitrogen) was applied. Quantitative PCR
455 was performed with target-specific primers using the TaqMan Gene Expression Assay (Applied
456 Biosystems) on an ABI Fast 7500 Sequence Detection System (Applied Biosystems) using the
457 following conditions: 95°C 20 sec, 40-45 cycles of the following: 95°C 3 sec, 60°C 30 sec. For lung
458 tissue and the BAL cellular fraction quantification was performed using AgPath-ID™ One-Step
459 RT-PCR Reagents (ThermoFisher), according to the manufacturer's instructions. The data were
460 analyzed using the SDS software (Applied Biosystems). Relative expression was calculated with
461 the ΔΔCT method [68]. The expression levels of the genes of interest, were normalized to the
462 housekeeping 18S rRNA. For the analysis of viral loads, RNA copy numbers were interpolated
463 from a standard curve generated with the serial dilution of a plasmid containing the cDNA of the
464 RSV L gene or the housekeeping 18S rRNA. The sequence of all the primers and probes is
465 summarized in **Table S3**.
466
467 **Flow cytometry**
468 FCM assays using different multicolor staining protocols were applied for the analysis of co-
469 stimulatory molecule expression and RSV infection of primary pediatric LR-MSCs, for the
470 identification and analysis of RSV infection of different cell types (AECs and LR-MSCs) in lung
471 cell suspensions derived from lambs, the assessment of apoptosis in the lung and the alveolar
472 space of infected and mock-infected animals. Further, a combination staining was applied to
473 evaluate the phenotype of cultured LR-MSCs. The detailed list of reagents used is summarized
474 in **Table S4**. FCM acquisitions were performed using a BD FACS Canto II (BD Bioscience) using
475 the DIVA software and were further analysed with the FlowJo software version 10.6.0 (BD). Dead
476 cells were excluded by electronic gating in forward/side scatter plots, followed by exclusion of
477 doublets as well as LIVE/DEAD® Fixable Dead Cell Staining (Invitrogen). Permeabilization and
478 fixation were undertaken according to the manufacturer's protocol (BD and Invitrogen).

479

480 **Trans-differentiation assay**

481 For differentiation, pediatric LR-MSCs (passage 5) and ovine LR-MSCs (passage 3) were plated
482 in a 24-well plate in regular culture medium and placed in a humidified atmosphere at 37°C with
483 5% CO_2. After 48 hours, cells were washed with PBS and complete differentiation media of the
484 different StemPro Differentiation Kits (Thermofisher) was added. For adipogenic induction cells
485 were plated at 10^4 cells/cm^2, for chondrogenic induction cells were plated at $2.7x10^4$ cells/cm^2,
486 and to induce osteogenic differentiation, cells were plated at $5x10^3$ cells/cm^2. Medium was
487 changed twice a week and after 15-21 days, cells were fixed with 4% PFA (Sigma). Adipocytes
488 were stained with Oil Red O (Sigma) to detect the formation of lipid droplets and counterstained
489 with hematoxylin (Carl Roth). Chondrocytes were stained with Alcian Blue (Sigma) to visualize
490 glycosaminoglycan synthesis and Alizarin Red S staining (Sigma) was used to detect Ca^{2+}
491 deposits in osteocytes.

492

493 **Microscopy analysis**

494 BAL-derived MSCs were cultured on a Nunc™ Lab-Tek™ II Chamber Slide™ System with 50'000
495 cells per chamber (ThermoFisher). Next, the cells were washed with cold PBS with Ca^{2+} and
496 incubated with Wheat Germ Agglutinin (WGA)-AF633 (Molecular Probes) for 10 min at 4°C. Then,
497 cells were fixed with 4% PFA for 10 min at room temperature. Next, the cells were washed with
498 0.3% saponin (Sigma) and stained with RSV-IgG(goat)-biotin antibody (Bio-Rad) for 20 min at
499 4°C. Then, 20 min incubation at 4°C with Strepta-AF546 was applied. Finally, DAPI (Sigma) was
500 added for 5 min at 37°C and cells were washed three times with cold PBS with Ca^{2+} before
501 mounting with MOWIOL® 4-88 Reagent (Sigma-Aldrich). Confocal microscopy analysis was
502 performed with a Nikon Eclipse Ti microscope (Nikon). All images were acquired using a 63X oil-
503 immersion objective. The images were analyzed with IMARIS 7.7 software (Bitplane) with
504 threshold subtraction and gamma correction. To monitor the spread of RSV-mCherry infection in
505 WD-AEC in comparison to MSC cultures, a Nikon BioStation CT was used (Nikon). The cultures
506 were followed over a period of 2 days with a 10X objective and images were acquired in an

507 automated sequence every 4 to 8 hours following infection. Reporter expression of RSV-mCherry-
508 infected pediatric LR-MSCs and ovine LR-MSCs was assessed using an Evos FL Auto 2 cell
509 imaging system (ThermoFisher) or a Leica TCS-SL, respectively. The micrographs from the trans-
510 differentiation assays were captured using an inverted microscope ECLIPSE TS100 with a Nikon
511 DS-Fi3 camera using a DS-L4 application v.1.5.03 (all form Nikon).
512
513 **Immunoassays**
514 When performing cytokine quantification, the supernatants and the basolateral medium from
515 RSV-A2 and RSV-ON1-H1 infections as well as of poly(I:C)-stimulated and unstimulated, and
516 mock-infected pediatric LR-MSCs and WD-AECs, respectively, were harvested after 24 and 72 h
517 of culture at 37°C with 5% CO_2. Human IFN-β, IFN-λ1/3 concentrations were determined using
518 commercial enzyme-linked immunosorbent assay (ELISA) kits (R&D Systems) following the
519 manufacturer's protocol. For the multiplex assay, the Pro™ Human Cytokine 27-plex Assay (Bio-
520 Rad) was used according to the manufacturer's protocol and read on a Bio-Plex 3D suspension
521 array system including a Bio-Plex Manager software v 6.0 (Bio-Rad).
522
523 **Animals**
524 The experiments with lambs were performed in compliance with the Swiss animal protection law
525 (TSchV SR 455.1; TVV SR 455.163). They were reviewed by the cantonal committee on animal
526 experiments of the canton of Bern, Switzerland and approved by the cantonal veterinary authority
527 with the license number BE125/17 (Amt für Landwirtschaft und Natur LANAT, Veterinärdienst
528 VeD, Bern, Switzerland). Newborn lambs, males and females were allocated randomly to different
529 groups (see below). Before and during the experiment, they were kept with their ewes. In order
530 to prevent secondary bacterial infections, the lambs received a prophylactic long-acting antibiotic
531 treatment by intramuscular injection of an oxytetracycline hydrochloride preparation (Cyclosol LA,
532 20 mg/kg) starting at 18 to 24 h before RSV infection. The treatment was repeated 2 times with 4
533 days interval. The trans-tracheal RSV inoculation was performed under sedation and analgesia
534 by intramuscular injection of a mixture of midazolam (Dormicum) 0.2 mg/kg and butorphanol

535 (Morphasol) 0.2 mg/kg. The trachea was punctured between the tracheal rings with a 0.9 x 40
536 mm needle (20G) and a volume of 2 ml of virus (10^8 PFU) or PBS (mock-infected controls) were
537 injected. Body temperature, body weight and clinical status (respiratory and heart rates) were
538 assessed daily by a veterinarian, whenever possible by the same person to ensure unbiased
539 clinical assessment. At defined time points, namely at 3, 6, 14, and 42 days p.i., the lambs were
540 euthanized and examined for gross- and histopathology. The lung was processed for *post-*
541 *mortem* bronchoalveolar lavage.
542
543 **Histopathological evaluation of lung tissue**
544 Lung specimens were fixed in 4% buffered formalin for 48 h, embedded in paraffin and routinely
545 processed for histology. Histological sections of 3 μm were stained with hematoxylin and eosin
546 coloration and observed by light microscopy.
547
548 **Processing of lung tissue and bronchoalveolar lavage**
549 One specimen per lung region (cranial, middle, and caudal) were pooled and dissociation was
550 done using a collagenase I and II and a DNase I enzyme mix (all from BioConcept) and the
551 gentleMACS Octo Dissociator (Miltenyi Biotec). Following this mechanical and enzymatical
552 dissociation, the samples were applied to a sieve, to remove any remaining particulate matter.
553 The cell suspensions were passed through cell strainers (100 and 70 µm pore-size, Falcon) and
554 centrifuged at 350g for 10 min at 4°C to obtain single-cell suspensions. For the isolation of cells
555 from BALs, the lungs were isolated with the trachea, which was clamped before cutting, to prevent
556 blood from entering the lungs. Then, a PBS-containing antibiotic solution with 100 units/ml of
557 penicillin and 100 µg/ml streptomycin (both Sigma), and 2.5 μg/ml Amphotericin B (ThermoFisher)
558 was poured into the lungs through a sterile funnel (200-500 ml). The cell suspensions were then
559 passed through cell strainers (100 and 70 µm pore-size, Falcon) and centrifuged at 350g for 10
560 min at 4°C to obtain single cell suspensions. If needed, red blood cells were lysed by
561 resuspending the pellet with 2 ml of H_2O and washed immediately in cold PBS before
562 centrifugation at 350g for 10 min at 4°C. Cells were then processed for FCM analysis, CFU-F

563 assay or expanded in culture to obtain lung-derived MSCs. To isolate and expand MSCs in
564 culture, lung cell suspensions were seeded at a density of $3.5x10^4$ cells per cm^2 in tissue culture
565 flasks as described previously [3]. Cells were maintained in α-MEM (Thermofisher) supplemented
566 with 10% FBS (ThermoFisher), an antibiotic solution containing 100 units/ml of penicillin and 100
567 µg/ml streptomycin, and 2.5 µg/ml Amphotericin B. After one to two days, the medium was
568 changed and cells were maintained at 37°C with 5% CO_2 until reaching ~80% of confluence.
569 Regular media changes were performed twice a week.
570
571 **Colony-forming unit-fibroblast assay**
572 Lung single-cell suspensions were seeded at a density of $3.5x10^4$ cells per cm^2 in a six-well plate
573 as described previously [3]. Cells were fixed after 7-14 days with ice-cold methanol for 20 min
574 and then washed with PBS. The cells were stained with Giemsa stain for 6 min, rinsed with H_2O,
575 and air-dried. Images were captured using an ImmunoSpot analyzer (CTL). Two experienced
576 investigators performed the CFU-F counts independently.
577
578 **RNA isolation and mRNA sequencing**
579 For mRNA sequencing, total RNA was extracted from ovine LR-MSCs using TRIzol reagent
580 (ThermoFisher) in combination with the Nucleospin RNA Kit (Machery-Nagel) as previously
581 described [69]. In short, cells were lysed with 1 ml of TRIzol reagent and kept at -70°C until further
582 processing. After thawing, 0.2 ml chloroform was added to the TRIzol lysate and the samples
583 were mixed vigorously and incubated for 2-3 min at room temperature. The extractions were then
584 centrifuged at 12'000g for 15 min at 4°C. The aqueous phase was collected and mixed with 500
585 µl 75% ethanol and the RNA precipitated for 10 min at room temperature. The RNA precipitate
586 was further purified with the Nucleospin RNA kit according to the manufacturer's instructions.
587 Quality and concentrations of the purified total RNA were assessed with an Agilent 2100
588 Bioanalyzer using a HS RNA (15nt) Kit (Agilent Technologies) and a Qubit 2.0 Fluorometer with
589 the Qubit RNA HS Assay Kit (ThermoFisher), respectively. Approximately 1 µg of high-quality
590 RNA (RNA integrity number >9) was used for paired-end mRNA library preparation (TruSeq

591 Sample Preparation Kit; Illumina). Total mRNA libraries were randomly multiplexed randomly in
592 eight samples per lane and sequenced on the NovaSeq 6000 System using the SP flow cell type
593 (Illumina) using paired-end sequencing cycles (100 cycles, 2x50 bp). All samples were run on the
594 same day. Quality control assessments, library preparation, and sequencing were all performed
595 at the Next Generation Sequencing Platform of the University of Bern, Switzerland. Analysis of
596 the RNA-seq data was performed at the Interfaculty Bioinformatics Unit at the University of Bern,
597 Switzerland. RNAseq data quality was assessed using fastqc v. 0.11.5 and RSeQC v. 2.6.4 [70].
598 The reads were mapped to the *Ovis aries* reference genome (Oar_v3.1) with Hisat2 v.2.1.0 [71].
599 To count the number of reads overlapping with each gene, as specified in the Ensembl annotation
600 FeatureCounts from Subread v.1.5.3 [72] was used. The Bioconductor package DESeq2 [73] was
601 applied to test for differential gene expression between the experimental groups. To evaluate
602 gene expression levels of MSC markers we applied the TPM normalization method [74]. The
603 molecular signatures database (MSigDB) with the Hallmark gene sets was used for gene set
604 enrichment analysis (GSEA) [75]. Analysis was done using R v.3.4.4 (2018-03-15).
605
606 **Statistical analysis**
607 The Prism 8 software (GraphPad) was used for statistical analysis. To determine differences
608 between two groups, non-parametric paired Wilcoxon test or Mann–Whitney U-test were used.
609 For multiple comparisons one-way ANOVA with Tukey post-hoc test or Kruskal-Wallis test with
610 Dunn's correction were used. A $p < 0.05$ was considered statistically significant.
611
612 **NOTES**
613 **Acknowledgment**
614 We are grateful to Sylvie Python and Aurélie Godel for technical assistance; Inês Margarida
615 Berenguer Veiga, Nathan Leborgne, Loic Borcard, Amal Fahmi and Charaf Benarafa for
616 participation in the animal trial; Hans-Peter Lüthi, Roman Troxler, Jan Salchli, Daniel Brechbühl,
617 Katarzyna Sliz, and Veronika Ayala for animal care. We thank Dominic Garcin for sharing the
618 RSV-mCherry construct. We thank Sibylle Haid, Martin Wetzke, Gesine Hansen, and Thomas

619 Pietschmann for sharing the RSV-ON1-H1 isolate. We thank Heidi Tschanz-Lischer, Irene Keller,
620 and Jenna Kelly for their bioinformatics support. We thank Christoph Aebi for helpful discussions.
621 We thank all study participants and their families. This work was supported by grants from the
622 Swiss National Science Foundation (project No. 310030_172895) and from the Bangerter-Rhyner
623 Foundation (both to MPA).

624

625 **Competing interest**

626 All the authors declare that they have no competing interests.

627

628 **Data availability statement**

629 The data generated and analyzed during the current study are available from the corresponding
630 author on reasonable request.

631

632 **Author's contributions**

633 Conception and design: MPA, MB. Collection of pediatric samples: UM, TMM, RAS, SRRH.
634 Acquisition of data: MB, BZ, TD, KM, NR, BIOE, QH, AS, SRRH. Contribution to reagents: MARW,
635 JFE. Analysis and interpretation: MPA, MB, KM, HP, GTB. Drafting the manuscript: MB, MPA.
636 Final approval of the manuscript: all authors.

637

638 **SUPPORTING INFORMATION**

639 Figure S1. PD-L1 and MHC class I surface expression in RSV-infected LR-MSCs

640 Figure S2. Characterization and RSV-infection of ovine LR-MSCs

641 Figure S3. Syncytium formation in neonatal lungs upon RSV infection

642 Figure S4. FCM assay for apoptosis detection *in vivo*

643 Figure S5. Targeting of AECs and LR-MSCs following neonatal RSV infection

644 Figure S6. Formation of syncytium upon RSV infection of human and ovine LR-MSCs

645 Table S1. List of significant DEGs in RSV infected *versus* mock-treated animals

646 Table S2. Patient characteristics

647 Table S3. List of qPCR primers

648 Table S4. List of antibodies used

649

650 **REFERENCES**

651 1. Crisan M, Yap S, Casteilla L, Chen CW, Corselli M, Park TS, et al. A perivascular origin
652 for mesenchymal stem cells in multiple human organs. Cell stem cell. 2008;3(3):301-13. doi:
653 10.1016/j.stem.2008.07.003. PubMed PMID: 18786417.

654 2. Hennrick KT, Keeton AG, Nanua S, Kijek TG, Goldsmith AM, Sajjan US, et al. Lung cells
655 from neonates show a mesenchymal stem cell phenotype. American journal of respiratory and
656 critical care medicine. 2007;175(11):1158-64. Epub 2007/03/03. doi: 10.1164/rccm.200607-
657 941OC. PubMed PMID: 17332484.

658 3. Lama VN, Smith L, Badri L, Flint A, Andrei AC, Murray S, et al. Evidence for tissue-resident
659 mesenchymal stem cells in human adult lung from studies of transplanted allografts. J Clin Invest.
660 2007;117(4):989-96. doi: 10.1172/JCI29713. PubMed PMID: 17347686; PubMed Central PMCID:
661 PMCPMC1810571.

662 4. Zepp JA, Zacharias WJ, Frank DB, Cavanaugh CA, Zhou S, Morley MP, et al. Distinct
663 Mesenchymal Lineages and Niches Promote Epithelial Self-Renewal and Myofibrogenesis in the
664 Lung. Cell. 2017;170(6):1134-48 e10. Epub 2017/09/09. doi: 10.1016/j.cell.2017.07.034. PubMed
665 PMID: 28886382; PubMed Central PMCID: PMCPMC5718193.

666 5. Lee JH, Tammela T, Hofree M, Choi J, Marjanovic ND, Han S, et al. Anatomically and
667 Functionally Distinct Lung Mesenchymal Populations Marked by Lgr5 and Lgr6. Cell.
668 2017;170(6):1149-63 e12. Epub 2017/09/09. doi: 10.1016/j.cell.2017.07.028. PubMed PMID:
669 28886383; PubMed Central PMCID: PMCPMC5607351.

670 6. Paris AJ, Hayer KE, Oved JH, Avgousti DC, Toulmin SA, Zepp JA, et al. STAT3-BDNF-
671 TrkB signalling promotes alveolar epithelial regeneration after lung injury. Nat Cell Biol.
672 2020;22(10):1197-210. Epub 2020/09/30. doi: 10.1038/s41556-020-0569-x. PubMed PMID:
673 32989251.

674 7. Xie T, Wang Y, Deng N, Huang G, Taghavifar F, Geng Y, et al. Single-Cell Deconvolution
675 of Fibroblast Heterogeneity in Mouse Pulmonary Fibrosis. Cell Rep. 2018;22(13):3625-40. Epub
676 2018/03/29. doi: 10.1016/j.celrep.2018.03.010. PubMed PMID: 29590628; PubMed Central
677 PMCID: PMCPMC5908225.

678 8. Beers MF, Morrisey EE. The three R's of lung health and disease: repair, remodeling, and
679 regeneration. J Clin Invest. 2011;121(6):2065-73. Epub 2011/06/03. doi: 10.1172/JCI45961.
680 PubMed PMID: 21633173; PubMed Central PMCID: PMCPMC3104764.

681 9. Aggarwal S, Pittenger MF. Human mesenchymal stem cells modulate allogeneic immune
682 cell responses. Blood. 2005;105(4):1815-22. Epub 2004/10/21. doi: 10.1182/blood-2004-04-
683 1559. PubMed PMID: 15494428.

684 10. Glassberg MK, Minkiewicz J, Toonkel RL, Simonet ES, Rubio GA, DiFede D, et al.
685 Allogeneic Human Mesenchymal Stem Cells in Patients With Idiopathic Pulmonary Fibrosis via
686 Intravenous Delivery (AETHER): A Phase I Safety Clinical Trial. Chest. 2017;151(5):971-81. Epub
687 2016/11/29. doi: 10.1016/j.chest.2016.10.061. PubMed PMID: 27890713; PubMed Central
688 PMCID: PMCPMC6026255.

689 11. Islam MN, Das SR, Emin MT, Wei M, Sun L, Westphalen K, et al. Mitochondrial transfer
690 from bone-marrow-derived stromal cells to pulmonary alveoli protects against acute lung injury.
691 Nat Med. 2012;18(5):759-65. Epub 2012/04/17. doi: 10.1038/nm.2736. PubMed PMID:
692 22504485; PubMed Central PMCID: PMCPMC3727429.

693 12. Villenave R, Thavagnanam S, Sarlang S, Parker J, Douglas I, Skibinski G, et al. In vitro
694 modeling of respiratory syncytial virus infection of pediatric bronchial epithelium, the primary
695 target of infection in vivo. Proceedings of the National Academy of Sciences of the United States
696 of America. 2012;109(13):5040-5. doi: 10.1073/pnas.1110203109. PubMed PMID: 22411804;
697 PubMed Central PMCID: PMC3323997.

698 13. Fonceca AM, Flanagan BF, Trinick R, Smyth RL, McNamara PS. Primary airway epithelial
699 cultures from children are highly permissive to respiratory syncytial virus infection. Thorax.
700 2012;67(1):42-8. Epub 2011/08/26. doi: 10.1136/thoraxjnl-2011-200131. PubMed PMID:
701 21865207.

702 14. Zhang L, Peeples ME, Boucher RC, Collins PL, Pickles RJ. Respiratory syncytial virus
703 infection of human airway epithelial cells is polarized, specific to ciliated cells, and without obvious
704 cytopathology. J Virol. 2002;76(11):5654-66. Epub 2002/05/07. doi: 10.1128/jvi.76.11.5654-
705 5666.2002. PubMed PMID: 11991994; PubMed Central PMCID: PMCPMC137037.

706 15. Falsey AR, Hennessey PA, Formica MA, Cox C, Walsh EE. Respiratory syncytial virus
707 infection in elderly and high-risk adults. N Engl J Med. 2005;352(17):1749-59. Epub 2005/04/29.
708 doi: 10.1056/NEJMoa043951. PubMed PMID: 15858184.

709 16. Coultas JA, Smyth R, Openshaw PJ. Respiratory syncytial virus (RSV): a scourge from
710 infancy to old age. Thorax. 2019;74(10):986-93. Epub 2019/08/07. doi: 10.1136/thoraxjnl-2018-
711 212212. PubMed PMID: 31383776.

712 17. Olivier A, Gallup J, de Macedo MM, Varga SM, Ackermann M. Human respiratory syncytial
713 virus A2 strain replicates and induces innate immune responses by respiratory epithelia of

714 neonatal lambs. Int J Exp Pathol. 2009;90(4):431-8. doi: 10.1111/j.1365-2613.2009.00643.x.
715 PubMed PMID: 19659901; PubMed Central PMCID: PMCPMC2741153.

716 18. Sitthicharoenchai P, Alnajjar S, Ackermann MR. A model of respiratory syncytial virus
717 (RSV) infection of infants in newborn lambs. Cell Tissue Res. 2020;380(2):313-24. Epub
718 2020/04/30. doi: 10.1007/s00441-020-03213-w. PubMed PMID: 32347384; PubMed Central
719 PMCID: PMCPMC7223741.

720 19. Altamirano-Lagos MJ, Diaz FE, Mansilla MA, Rivera-Perez D, Soto D, McGill JL, et al.
721 Current Animal Models for Understanding the Pathology Caused by the Respiratory Syncytial
722 Virus. Front Microbiol. 2019;10:873. Epub 2019/05/28. doi: 10.3389/fmicb.2019.00873. PubMed
723 PMID: 31130923; PubMed Central PMCID: PMCPMC6510261.

724 20. Dominici M, Le Blanc K, Mueller I, Slaper-Cortenbach I, Marini F, Krause D, et al. Minimal
725 criteria for defining multipotent mesenchymal stromal cells. The International Society for Cellular
726 Therapy position statement. Cytotherapy. 2006;8(4):315-7. Epub 2006/08/23. doi:
727 10.1080/14653240600855905. PubMed PMID: 16923606.

728 21. Evelyn A. Kurt-Jones LP, Laura Kwinn, Lia M. Haynes, Les P. Jones,, Ralph A.Tripp EEW,
729 Mason W. Freeman, Douglas T. Golenbock,, Finberg LJAaRW. Pattern recognition receptors
730 TLR4 and CD14 mediate response to respiratory syncytial virus. Nature Immunology. 2000;1.

731 22. Behera AK, Matsuse H, Kumar M, Kong X, Lockey RF, Mohapatra SS. Blocking
732 intercellular adhesion molecule-1 on human epithelial cells decreases respiratory syncytial virus
733 infection. Biochem Biophys Res Commun. 2001;280(1):188-95. Epub 2001/02/13. doi:
734 10.1006/bbrc.2000.4093. PubMed PMID: 11162498.

735 23. Malhotra R, Ward M, Bright H, Priest R, Foster Martyn R, Hurle M, et al. Isolation and
736 characterisation of potential respiratory syncytial virus receptor(s) on epithelial cells. Microbes
737 and Infection. 2003;5(2):123-33. doi: 10.1016/s1286-4579(02)00079-5.

738 24. Tayyari F, Marchant D, Moraes TJ, Duan W, Mastrangelo P, Hegele RG. Identification of
739 nucleolin as a cellular receptor for human respiratory syncytial virus. Nature medicine.
740 2011;17(9):1132-5. doi: 10.1038/nm.2444. PubMed PMID: 21841784.

741 25. Schoggins JW, Rice CM. Interferon-stimulated genes and their antiviral effector functions.
742 Curr Opin Virol. 2011;1(6):519-25. Epub 2012/02/14. doi: 10.1016/j.coviro.2011.10.008. PubMed
743 PMID: 22328912; PubMed Central PMCID: PMCPMC3274382.

744 26. Bichsel CA, Wang L, Froment L, Berezowska S, Muller S, Dorn P, et al. Increased PD-L1
745 expression and IL-6 secretion characterize human lung tumor-derived perivascular-like cells that

746 promote vascular leakage in a perfusable microvasculature model. Sci Rep. 2017;7(1):10636.
747 Epub 2017/09/08. doi: 10.1038/s41598-017-09928-1. PubMed PMID: 28878242; PubMed
748 Central PMCID: PMCPMC5587684.

749 27. Klyushnenkova E, Mosca JD, Zernetkina V, Majumdar MK, Beggs KJ, Simonetti DW, et
750 al. T cell responses to allogeneic human mesenchymal stem cells: immunogenicity, tolerance,
751 and suppression. J Biomed Sci. 2005;12(1):47-57. Epub 2005/05/03. doi: 10.1007/s11373-004-
752 8183-7. PubMed PMID: 15864738.

753 28. McCarty RC, Gronthos S, Zannettino AC, Foster BK, Xian CJ. Characterisation and
754 developmental potential of ovine bone marrow derived mesenchymal stem cells. J Cell Physiol.
755 2009;219(2):324-33. doi: 10.1002/jcp.21670. PubMed PMID: 19115243.

756 29. Zhao S, Tao L, Tian Y, Tai D, Liu P, Liu D. Isolation and characterization of ovine umbilical
757 cord-derived mesenchymal stem cells. Cytotechnology. 2019;71(1):277-86. Epub 2019/01/04.
758 doi: 10.1007/s10616-018-0284-7. PubMed PMID: 30603926; PubMed Central PMCID:
759 PMCPMC6368499.

760 30. Jakub Grzesiak KM, Karol Wrzeszcz, Joanna Czogała. Isolation and Morphological
761 Characterisation of Ovine Adipose-Derived Mesenchymal Stem Cells in Culture. International
762 Journal of Stem Cells. 2011;4.

763 31. O'Connor K. A cautionary tale about the use of colony-forming efficiency as a proxy for
764 the survival of mesenchymal stem cells. Stem Cell Res Ther. 2020;11(1):292. Epub 2020/07/18.
765 doi: 10.1186/s13287-020-01805-5. PubMed PMID: 32678014.

766 32. Friedenstein AJ, Chailakhjan RK, Lalykina KS. The development of fibroblast colonies in
767 monolayer cultures of guinea-pig bone marrow and spleen cells. Cell Tissue Kinet. 1970;3(4):393-
768 403. Epub 1970/10/01. doi: 10.1111/j.1365-2184.1970.tb00347.x. PubMed PMID: 5523063.

769 33. Spadafora R, Lu J, Khetani RS, Zhang C, Iberg A, Li H, et al. Lung-Resident Mesenchymal
770 Stromal Cells Reveal Transcriptional Dynamics of Lung Development in Preterm Infants.
771 American journal of respiratory and critical care medicine. 2018;198(7):961-4. Epub 2018/05/15.
772 doi: 10.1164/rccm.201801-0024LE. PubMed PMID: 29757681; PubMed Central PMCID:
773 PMCPMC6173067.

774 34. Rohart F, Mason EA, Matigian N, Mosbergen R, Korn O, Chen T, et al. A molecular
775 classification of human mesenchymal stromal cells. PeerJ. 2016;4:e1845. Epub 2016/04/05. doi:
776 10.7717/peerj.1845. PubMed PMID: 27042394; PubMed Central PMCID: PMCPMC4811172.

777 35. Sattentau Q. Avoiding the void: cell-to-cell spread of human viruses. Nat Rev Microbiol.
778 2008;6(11):815-26. Epub 2008/10/17. doi: 10.1038/nrmicro1972. PubMed PMID: 18923409.

779 36. Wahl A, De C, Abad Fernandez M, Lenarcic EM, Xu Y, Cockrell AS, et al. Precision mouse
780 models with expanded tropism for human pathogens. Nat Biotechnol. 2019;37(10):1163-73. Epub
781 2019/08/28. doi: 10.1038/s41587-019-0225-9. PubMed PMID: 31451733; PubMed Central
782 PMCID: PMCPMC6776695.

783 37. Jain N, Kalam H, Singh L, Sharma V, Kedia S, Das P, et al. Mesenchymal stem cells offer
784 a drug-tolerant and immune-privileged niche to Mycobacterium tuberculosis. Nat Commun.
785 2020;11(1):3062. Epub 2020/06/18. doi: 10.1038/s41467-020-16877-3. PubMed PMID:
786 32546788; PubMed Central PMCID: PMCPMC7297998.

787 38. Eisenhut M. Extrapulmonary manifestations of severe respiratory syncytial virus infection-
788 -a systematic review. Crit Care. 2006;10(4):R107. Epub 2006/07/25. doi: 10.1186/cc4984.
789 PubMed PMID: 16859512; PubMed Central PMCID: PMCPMC1751022.

790 39. Rezaee F, Gibson LF, Piktel D, Othumpangat S, Piedimonte G. Respiratory syncytial virus
791 infection in human bone marrow stromal cells. Am J Respir Cell Mol Biol. 2011;45(2):277-86.
792 Epub 2010/10/26. doi: 10.1165/rcmb.2010-0121OC. PubMed PMID: 20971883; PubMed Central
793 PMCID: PMCPMC3175557.

794 40. Cheung MB, Sampayo-Escobar V, Green R, Moore ML, Mohapatra S, Mohapatra SS.
795 Respiratory Syncytial Virus-Infected Mesenchymal Stem Cells Regulate Immunity via Interferon
796 Beta and Indoleamine-2,3-Dioxygenase. PloS one. 2016;11(10):e0163709. Epub 2016/10/04.
797 doi: 10.1371/journal.pone.0163709. PubMed PMID: 27695127; PubMed Central PMCID:
798 PMCPMC5047639.

799 41. Heinonen S, Velazquez VM, Ye F, Mertz S, Acero-Bedoya S, Smith B, et al. Immune
800 profiles provide insights into respiratory syncytial virus disease severity in young children. Sci
801 Transl Med. 2020;12(540). Epub 2020/04/24. doi: 10.1126/scitranslmed.aaw0268. PubMed
802 PMID: 32321862.

803 42. Siefker DT, Vu L, You D, McBride A, Taylor R, Jones TL, et al. Respiratory Syncytial Virus
804 Disease Severity Is Associated with Distinct CD8(+) T-Cell Profiles. American journal of
805 respiratory and critical care medicine. 2020;201(3):325-34. Epub 2019/10/24. doi:
806 10.1164/rccm.201903-0588OC. PubMed PMID: 31644878; PubMed Central PMCID:
807 PMCPMC6999109.

808 43. Besteman SB, Callaghan A, Langedijk AC, Hennus MP, Meyaard L, Mokry M, et al.
809 Transcriptome of airway neutrophils reveals an interferon response in life-threatening respiratory

810 syncytial virus infection. Clin Immunol. 2020;220:108593. Epub 2020/09/14. doi:
811 10.1016/j.clim.2020.108593. PubMed PMID: 32920212.

812 44. Bradley KC, Finsterbusch K, Schnepf D, Crotta S, Llorian M, Davidson S, et al. Microbiota-
813 Driven Tonic Interferon Signals in Lung Stromal Cells Protect from Influenza Virus Infection. Cell
814 Rep. 2019;28(1):245-56 e4. Epub 2019/07/04. doi: 10.1016/j.celrep.2019.05.105. PubMed PMID:
815 31269444.

816 45. Tisoncik JR, Korth MJ, Simmons CP, Farrar J, Martin TR, Katze MG. Into the eye of the
817 cytokine storm. Microbiol Mol Biol Rev. 2012;76(1):16-32. Epub 2012/03/07. doi:
818 10.1128/mmbr.05015-11. PubMed PMID: 22390970; PubMed Central PMCID:
819 PMCPMC3294426.

820 46. McNamara PS, Flanagan BF, Hart CA, Smyth RL. Production of chemokines in the lungs
821 of infants with severe respiratory syncytial virus bronchiolitis. The Journal of infectious diseases.
822 2005;191(8):1225-32. Epub 2005/03/19. doi: 10.1086/428855. PubMed PMID: 15776367.

823 47. Rolandsson Enes S, Andersson Sjöland A, Skog I, Hansson L, Larsson H, Le Blanc K, et
824 al. MSC from fetal and adult lungs possess lung-specific properties compared to bone marrow-
825 derived MSC. Sci Rep. 2016;6:29160. Epub 2016/07/07. doi: 10.1038/srep29160. PubMed PMID:
826 27381039; PubMed Central PMCID: PMCPMC4933903.

827 48. Nordgren SNSaTM. Lung-Resident Mesenchymal Stromal Cells are Tissue-Specific
828 Regulators of Lung Homeostasis. ajp lung cellular and molecular physiology. 2020.

829 49. Kasahara Y, Tuder RM, Taraseviciene-Stewart L, Le Cras TD, Abman S, Hirth PK, et al.
830 Inhibition of VEGF receptors causes lung cell apoptosis and emphysema. J Clin Invest.
831 2000;106(11):1311-9. Epub 2000/12/06. doi: 10.1172/jci10259. PubMed PMID: 11104784;
832 PubMed Central PMCID: PMCPMC387249.

833 50. Aschner Y, Downey GP. Transforming Growth Factor-β: Master Regulator of the
834 Respiratory System in Health and Disease. American journal of respiratory cell and molecular
835 biology. 2016;54(5):647-55. Epub 2016/01/23. doi: 10.1165/rcmb.2015-0391TR. PubMed PMID:
836 26796672; PubMed Central PMCID: PMCPMC4942197.

837 51. Vaughan AE, Chapman HA. Regenerative activity of the lung after epithelial injury.
838 Biochim Biophys Acta. 2013;1832(7):922-30. Epub 2012/12/12. doi:
839 10.1016/j.bbadis.2012.11.020. PubMed PMID: 23219956.

840 52. Boregowda SV, Krishnappa V, Strivelli J, Haga CL, Booker CN, Phinney DG. Basal p53
841 expression is indispensable for mesenchymal stem cell integrity. Cell Death Differ.

842 2018;25(4):679-92. Epub 2018/01/10. doi: 10.1038/s41418-017-0004-4. PubMed PMID:
843 29311623; PubMed Central PMCID: PMCPMC5883824.

844 53. Phan SH. Genesis of the myofibroblast in lung injury and fibrosis. Proc Am Thorac Soc.
845 2012;9(3):148-52. Epub 2012/07/18. doi: 10.1513/pats.201201-011AW. PubMed PMID:
846 22802289; PubMed Central PMCID: PMCPMC5830705.

847 54. Respiratory Syncytial Virus and Recurrent Wheeze in Healthy Preterm Infants. N Engl J
848 Med. 2016;374(24):2406. Epub 2016/06/16. doi: 10.1056/NEJMx160016. PubMed PMID:
849 27305208.

850 55. Miller EK, Avila PC, Khan YW, Word CR, Pelz BJ, Papadopoulos NG, et al. Wheezing
851 exacerbations in early childhood: evaluation, treatment, and recent advances relevant to the
852 genesis of asthma. J Allergy Clin Immunol Pract. 2014;2(5):537-43. Epub 2014/09/13. doi:
853 10.1016/j.jaip.2014.06.024. PubMed PMID: 25213046; PubMed Central PMCID:
854 PMCPMC4190166.

855 56. Millar JE, Bartnikowski N, Passmore MR, Obonyo NG, Malfertheiner MV, von Bahr V, et
856 al. Combined Mesenchymal Stromal Cell Therapy and Extracorporeal Membrane Oxygenation in
857 Acute Respiratory Distress Syndrome. A Randomized Controlled Trial in Sheep. American journal
858 of respiratory and critical care medicine. 2020;202(3):383-92. Epub 2020/04/16. doi:
859 10.1164/rccm.201911-2143OC. PubMed PMID: 32293914; PubMed Central PMCID:
860 PMCPMC7397785.

861 57. Zumla A, Rao M, Wallis RS, Kaufmann SH, Rustomjee R, Mwaba P, et al. Host-directed
862 therapies for infectious diseases: current status, recent progress, and future prospects. Lancet
863 Infect Dis. 2016;16(4):e47-63. Epub 2016/04/03. doi: 10.1016/s1473-3099(16)00078-5. PubMed
864 PMID: 27036359; PubMed Central PMCID: PMCPMC7164794.

865 58. Chan MC, Kuok DI, Leung CY, Hui KP, Valkenburg SA, Lau EH, et al. Human
866 mesenchymal stromal cells reduce influenza A H5N1-associated acute lung injury in vitro and in
867 vivo. Proceedings of the National Academy of Sciences of the United States of America.
868 2016;113(13):3621-6. Epub 2016/03/16. doi: 10.1073/pnas.1601911113. PubMed PMID:
869 26976597; PubMed Central PMCID: PMCPMC4822574.

870 59. Khoury M, Cuenca J, Cruz FF, Figueroa FE, Rocco PRM, Weiss DJ. Current status of cell-
871 based therapies for respiratory virus infections: applicability to COVID-19. The European
872 respiratory journal. 2020;55(6). Epub 2020/04/09. doi: 10.1183/13993003.00858-2020. PubMed
873 PMID: 32265310; PubMed Central PMCID: PMCPMC7144273 IT16I10084), during the conduct
874 of the study; stipend received from Cells for Cells, outside the submitted work; has patents
875 WO2014135924A1 pending, WO2017064670A2 pending, WO2017064672A1 pending and

876 WO/2019/051623 pending; and is CSO of Cells for Cells, a University spin-off developing
877 therapies for osteoarthritis, pulpitis and cardiac failure, and Regenero, a consortium for Chilean
878 regenerative medicine (public and private funding), for skin ulcer and Lupus. Conflict of interest:
879 J. Cuenca reports grants from CONICYT (FONDEF 2016, IT16I10084), during the conduct of the
880 study; stipend received from Cells for Cells, outside the submitted work; and is a research scientist
881 for Cells for Cells, a University spin-off developing therapies for osteoarthritis, pulpitis and cardiac
882 failure, and Regenero, a consortium for Chilean regenerative medicine (public and private
883 funding), for skin ulcer and Lupus. Conflict of interest: F.F. Cruz has nothing to disclose. Conflict
884 of interest: F.E. Figueroa has a patent WO/2019/051623 pending and is a board member of Cells
885 for Cells, as the director of the programme of translational cell therapy at Universidad de los
886 Andes, the academic institution that originated the Consorcio Corfo Regenero and the Cells for
887 Cells biotechnological spin-off. Conflict of interest: P.R.M. Rocco has nothing to disclose. Conflict
888 of interest: D.J. Weiss reports grants from NIH, Cystic Fibrosis Foundation and US Department
889 of Defense, outside the submitted work.

890 60. Saldanha-Araujo F, Melgaço Garcez E, Silva-Carvalho AE, Carvalho JL. Mesenchymal
891 Stem Cells: A New Piece in the Puzzle of COVID-19 Treatment. Front Immunol. 2020;11:1563.
892 Epub 2020/07/29. doi: 10.3389/fimmu.2020.01563. PubMed PMID: 32719683; PubMed Central
893 PMCID: PMCPMC7347794.

894 61. Liang B, Chen J, Li T, Wu H, Yang W, Li Y, et al. Clinical remission of a critically ill COVID-
895 19 patient treated by human umbilical cord mesenchymal stem cells: A case report. Medicine
896 (Baltimore). 2020;99(31):e21429. Epub 2020/08/07. doi: 10.1097/md.0000000000021429.
897 PubMed PMID: 32756149; PubMed Central PMCID: PMCPMC7402800.

898 62. Guo Z, Chen Y, Luo X, He X, Zhang Y, Wang J. Administration of umbilical cord
899 mesenchymal stem cells in patients with severe COVID-19 pneumonia. Crit Care.
900 2020;24(1):420. Epub 2020/07/13. doi: 10.1186/s13054-020-03142-8. PubMed PMID: 32653043;
901 PubMed Central PMCID: PMCPMC7351637.

902 63. Thanunchai M, Hongeng S, Thitithanyanont A. Mesenchymal Stromal Cells and Viral
903 Infection. Stem Cells Int. 2015;2015:860950. Epub 2015/08/22. doi: 10.1155/2015/860950.
904 PubMed PMID: 26294919; PubMed Central PMCID: PMCPMC4532961.

905 64. Scheerlinck JP, Snibson KJ, Bowles VM, Sutton P. Biomedical applications of sheep
906 models: from asthma to vaccines. Trends Biotechnol. 2008;26(5):259-66. Epub 2008/03/21. doi:
907 10.1016/j.tibtech.2008.02.002. PubMed PMID: 18353472.

908 65. Wang L, Dorn P, Zeinali S, Froment L, Berezowska S, Kocher GJ, et al. CD90+CD146+
909 identifies a pulmonary mesenchymal cell subtype with both immune modulatory and perivascular-

910 like function in postnatal human lung. Am J Physiol Lung Cell Mol Physiol. 2020. doi:
911 10.1152/ajplung.00146.2019.

912 66. Rameix-Welti MA, Le Goffic R, Hervé PL, Sourimant J, Rémot A, Riffault S, et al.
913 Visualizing the replication of respiratory syncytial virus in cells and in living mice. Nat Commun.
914 2014;5:5104. Epub 2014/10/04. doi: 10.1038/ncomms6104. PubMed PMID: 25277263; PubMed
915 Central PMCID: PMCPMC7091779.

916 67. Blockus S, Sake SM, Wetzke M, Grethe C, Graalmann T, Pils M, et al. Labyrinthopeptins
917 as virolytic inhibitors of respiratory syncytial virus cell entry. Antiviral Res. 2020;177:104774. Epub
918 2020/03/22. doi: 10.1016/j.antiviral.2020.104774. PubMed PMID: 32197980.

919 68. Alves MP, Neuhaus V, Guzylack-Piriou L, Ruggli N, McCullough KC, Summerfield A. Toll-
920 like receptor 7 and MyD88 knockdown by lentivirus-mediated RNA interference to porcine
921 dendritic cell subsets. Gene Ther. 2007;14(10):836-44. PubMed PMID: 17330086.

922 69. Auray G, Keller I, Python S, Gerber M, Bruggmann R, Ruggli N, et al. Characterization
923 and Transcriptomic Analysis of Porcine Blood Conventional and Plasmacytoid Dendritic Cells
924 Reveals Striking Species-Specific Differences. J Immunol. 2016;197(12):4791-806. Epub
925 2016/11/12. doi: 10.4049/jimmunol.1600672. PubMed PMID: 27837108.

926 70. Wang L, Wang S, Li W. RSeQC: quality control of RNA-seq experiments. Bioinformatics.
927 2012;28(16):2184-5. Epub 2012/06/30. doi: 10.1093/bioinformatics/bts356. PubMed PMID:
928 22743226.

929 71. Kim D, Langmead B, Salzberg SL. HISAT: a fast spliced aligner with low memory
930 requirements. Nat Methods. 2015;12(4):357-60. Epub 2015/03/10. doi: 10.1038/nmeth.3317.
931 PubMed PMID: 25751142; PubMed Central PMCID: PMCPMC4655817.

932 72. Liao Y, Smyth GK, Shi W. featureCounts: an efficient general purpose program for
933 assigning sequence reads to genomic features. Bioinformatics. 2014;30(7):923-30. Epub
934 2013/11/15. doi: 10.1093/bioinformatics/btt656. PubMed PMID: 24227677.

935 73. Love MI, Huber W, Anders S. Moderated estimation of fold change and dispersion for
936 RNA-seq data with DESeq2. Genome Biol. 2014;15(12):550. Epub 2014/12/18. doi:
937 10.1186/s13059-014-0550-8. PubMed PMID: 25516281; PubMed Central PMCID:
938 PMCPMC4302049.

939 74. Wagner GP, Kin K, Lynch VJ. Measurement of mRNA abundance using RNA-seq data:
940 RPKM measure is inconsistent among samples. Theory Biosci. 2012;131(4):281-5. Epub
941 2012/08/09. doi: 10.1007/s12064-012-0162-3. PubMed PMID: 22872506.

75. Liberzon A, Birger C, Thorvaldsdóttir H, Ghandi M, Mesirov JP, Tamayo P. The Molecular Signatures Database (MSigDB) hallmark gene set collection. Cell Syst. 2015;1(6):417-25. Epub 2016/01/16. doi: 10.1016/j.cels.2015.12.004. PubMed PMID: 26771021; PubMed Central PMCID: PMCPMC4707969.

948 **FIGURE LEGENDS**

949 **Figure 1**: **LR-MSCs are highly permissive to RSV infection**

950 (A) Representative histograms showing expression of the surface markers CD73, CD90, CD105
951 on pediatric LR-MSCs. (B) Representative phase-contrast (PC) micrograph showing morphology
952 in culture and demonstrates plastic adherence. Representative images of Toluidine blue, Alizarin
953 Red S, and Oil Red O stainings after chondrogenic (C), osteogenic (O), and adipogenic (A)
954 differentiation, respectively. Magnification 40X (PC, O) and 200X (C, A). (C) mRNA expression
955 levels of RSV receptors relative to 10^6 18S. A Mann-Whitney U test was applied to compare the
956 two cell types (AECs *versus* LR-MSCs). Boxplots indicate the median value (centerline) and
957 interquartile ranges (box edges), with whiskers extending to the lowest and the highest values.
958 Each symbol represents an individual donor (n=5). *$p<0.05$, **$p<0.01$. (D) Viral loads in AECs
959 and LR-MSCs over time following infection with RSV-A2 at a MOI of 1 PFU/cell expressed as
960 RSV copies per 10^{12} 18S copies. Each symbol represents an individual donor (n=5). (E) RSV F-
961 protein positive LR-MSCs assessed by FCM and plotted over time. LR-MSCs were infected with
962 1-2 PFU/cell with RSV-A2 (n=3) or a clinical isolate RSV-ON1-H1 (n=6). Each symbol represents
963 an individual donor. (F) Representative live-cell imaging of AECs and LR-MSCs infected with 0.1-
964 0.5 PFU/cell with RSV-mCHerry and followed over time. The micrographs were taken at 16, 32,
965 and 48 h p.i. in the same area of the cellular layer (G, H) Supernatants of infected LR-MSCs or
966 apical washes of infected WD-AEC cultures were analyzed by a PFU assay. Cells were infected
967 with 0.1 (G) or 1 PFU/cell (H). A Mann-Whitney U test was applied to compare the two cell types
968 (WD-AECs, n=3 *versus* LR-MSCs, n=6). Each symbol represents an individual donor. *$p<0.05$,
969 **$p<0.01$.

970

971 **Figure 2: RSV infection is altering the immune properties of LR-MSCs**

972 (A, B) mRNA levels of selected ISGs (A) and IFNs (B) in LR-MSCs treated with mock control,
973 poly(I:C) 10 μg/ml, RSV-A2, or RSV-ON1-H1 for 24 h at 1 PFU/cell. Boxplots indicate the median
974 value (centerline) and interquartile ranges (box edges), with whiskers extending to the lowest and
975 the highest values. Each symbol represents an individual donor (mock, n=6; poly(I:C), n=5; RSV

976 A2, n=4; RSV-ON1-H1, n=6). The data were compared with the Kruskal–Wallis test followed by
977 Dunn's post hoc test. *p<0.05, **p<0.01. (C, D) IFN-β (C) and IFN-λ1/3 (D) protein levels in
978 supernatants of LR-MSCs treated with mock control, poly(I:C) 10 μg/ml, RSV-A2, or RSV-ON1-
979 H1 for 24 h and 72 h at 1 PFU/cell. Boxplots indicate median value (centerline) and interquartile
980 ranges (box edges), with whiskers extending to the lowest and the highest values. Each symbol
981 represents an individual donor (mock, n=6; poly(I:C), n=5; RSV A2, n=4; RSV-ON1-H1, n=6). A
982 Kruskal–Wallis test followed by a Dunn's post hoc test was applied to compare the different
983 groups. *p<0.05, **p<0.01, ***p<0.001. The detection limits of the assays are indicated with the
984 dotted line at 7.7 pg/mL and 93.3 pg/mL for IFN-β and IFN-λ1/3, respectively. (E, F) Multiplex
985 assay of supernatants of LR-MSCs (E) or basolateral medium of WD-AECs (F), 24 and 72h after
986 treatment with mock control, 10 μg/ml poly(I:C), RSV-A2, or RSV-ON1-H1 for 24h and 72h at 1
987 PFU/cell. The concentration ranges of the different cytokines are indicated (lower detection limit-
988 highest concentration measured). An asterisk is present when the concentration of the sample
989 was higher than the upper range of the assay. Each column represents a different donor (mock,
990 n=6; poly(I:C), n=5; RSV A2, n=4; RSV-ON1-H1, n=6). (donors a-c for WD-AECs and d-i for LR-
991 MSCs). (G) Overview of the impact of RSV infection of LR-MSCs activity. RSV-mediated
992 activation of LR-MSCs, characterized by an antiviral and pro-inflammatory phenotype combined
993 with cytokines promoting T helper cell (Th) polarization.
994
995 **Figure 3**: **RSV infection is causing lung injury in lamb**
996 (A) Newborn animals were trans-tracheally inoculated with 10^8 PFU per animal of the human
997 strain RSV-A2 or PBS (mock). Animals were euthanized 3, 6, 14, and 42 days p.i. and lung and
998 BAL tissues were harvested for histopathological evaluation, qPCR, and FCM analysis (B)
999 Representative H&E stained histopathological sections of the lung tissue from noninfected (mock)
1000 and RSV-infected lambs at 3, 6, 14, and 42 days p.i. Scale bar, 200 μm. (C) Viral load in lungs
1001 and the cellular fraction of the BAL of infected lambs measured 3, 6, 14, and 42 days p.i.
1002 Comparison of viral loads between BAL and lung tissues was done with a one-way ANOVA and

1003 the Tukey post-hoc test. Each symbol represents an individual animal (n=6 per timepoint).
1004 *p<0.05. (D, E) Frequency of cleaved caspase 3 (CASP3)-positive cells in the lung (D) and BAL
1005 (E) of infected animals 3 to 42 days p.i. Boxplots indicate the median value (centerline) and
1006 interquartile ranges (box edges), with whiskers extending to the lowest and the highest values.
1007 Each symbol represents an individual animal (mock, n=3 and RSV, n=6). Multiple comparison
1008 was done with a one-way ANOVA and the Tukey post-hoc test. *p<0.05. (F) Total BAL cell counts
1009 in mock and RSV-infected animals 3, 6, and 14 days p.i. pooled. Boxplots indicate the median
1010 value (centerline) and interquartile ranges (box edges), with whiskers extending to the lowest and
1011 the highest values. Each symbol represents an individual animal (n=9, mock and n=18, RSV). A
1012 Mann-Whitney U test was applied to compare the two groups. **p<0.01.
1013
1014 **Figure 4**: **LR-MSCs are a target for RSV infection *in vivo***
1015 (A) FCM gating strategy to identify RSV-infected epithelial cells ($CD31^-CD45^-panCTK^+$) (panCTK,
1016 pan-cytokeratin) and LR-MSCs ($CD31^-CD45^-panCTK\text{-}CD29^+CD44^+$). (G1, gate 1) (B) Percentage
1017 of animals with RSV-positive epithelial and LR-MSCs 3 to 42 days p.i. The fractions indicate the
1018 number of infected animals where infection was detected by FCM compared to the total number
1019 of animals. (C) Correlation of RSV-positive LR-MSCs and RSV-positive epithelial cells at 3 and 6
1020 days p.i. Associations were tested using the Spearman rank correlation test. Each symbol
1021 represents an individual animal. (D) RSV loads in MSCs isolated from lung and BAL tissues of
1022 RSV-infected animals 3, 6, 14, and 42 d p.i. and expanded in culture. Each symbol represents an
1023 individual animal (n=6-8). (E) Phase-contrast micrographs of LR-MSCs derived from BALs
1024 expanded in culture from noninfected (mock) or infected (RSV) animals 3 days p.i. Magnification
1025 100X. (F) Representative confocal microscopy evaluation of LR-MSCs derived from BALs
1026 expanded in culture from noninfected (mock) or infected (RSV) animals 3 days p.i. RSV, orange;
1027 DAPI, dark blue; WGA, light blue. Scale bars, 15 µm and 10 µm for the 3D capture.
1028
1029 **Figure 5: RSV infection leads to the expansion of the pulmonary MSC niche *in vivo***

1030 (A) Newborn or adult (average age of 29 months) animals were trans-tracheally inoculated with
1031 10^8 PFU per animal of the human strain RSV-A2 or PBS (mock). Newborns were euthanized 3,
1032 6, 14, and 42 days p.i. and adults 6 and 14 days p.i. and lung tissue was harvested for CFU-F
1033 assay. Lung tissue of adults was harvested for histopathological evaluation (B) Representative
1034 H&E stained histopathological sections of the lung tissue from noninfected (mock) and RSV-
1035 infected adults at 6 and 14 days p.i. scale bar, 200 µm. (C, E) Representative images of the CFU-
1036 F assay for mock control and RSV-infected neonates (C) and adults (E) 3 to 42 days p.i. and 6
1037 and 14 days p.i., respectively. Each image represents an individual animal. (D, F) Quantification
1038 of the CFU-F assay for each neonate (D) and adult (F) animals, given as CFU-F count relative to
1039 $3.33X10^5$ nucleated cells over time. Boxplots indicate the median value (centerline) and
1040 interquartile ranges (box edges), with whiskers extending to the lowest and the highest values.
1041 Each symbol represents an individual animal (neonates, per timepoint: mock, n=3-4; RSV, n=6-
1042 8; adults: mock, n=14; RSV, n=3 per timepoint). A one-way ANOVA and the Holm-Sydak post-
1043 hoc test was applied to compare differences between groups. *p<0.05, ***p<0.001, ****p<0.0001.
1044

1045 **Figure 6: The transcriptional activity of LR-MSCs is related to the phases of RSV disease**
1046 (A) Expression levels of selected classical MSC markers expressed as log_2TPM (TPM, transcripts
1047 per million). Each column is a different time p.i. (B-D) Volcano plot of the DEGs from the
1048 comparison of RSV infection and mock control 6 (B), 14 (C), and 42 (D) days p.i. with p_{adj}<0.05
1049 (red filed circles). (B) Pie chart with the 14 DEGs (p_{adj}<0.05) categorized according to their
1050 function. (D) Pie chart with the 43 DEGs (p_{adj}<0.05) categorized according to their function. (E)
1051 Normalized enrichment score of significant (false discovery rate, FDR<0.05) hallmark gene sets
1052 for the comparisons of RSV infection and mock control 6, 14, and 42 days p.i. (downregulated,
1053 blue and upregulated, red) (F) Cartoon summarizing the different functions of LR-MSCs during
1054 distinct steps of RSV disease.

Fig. 1

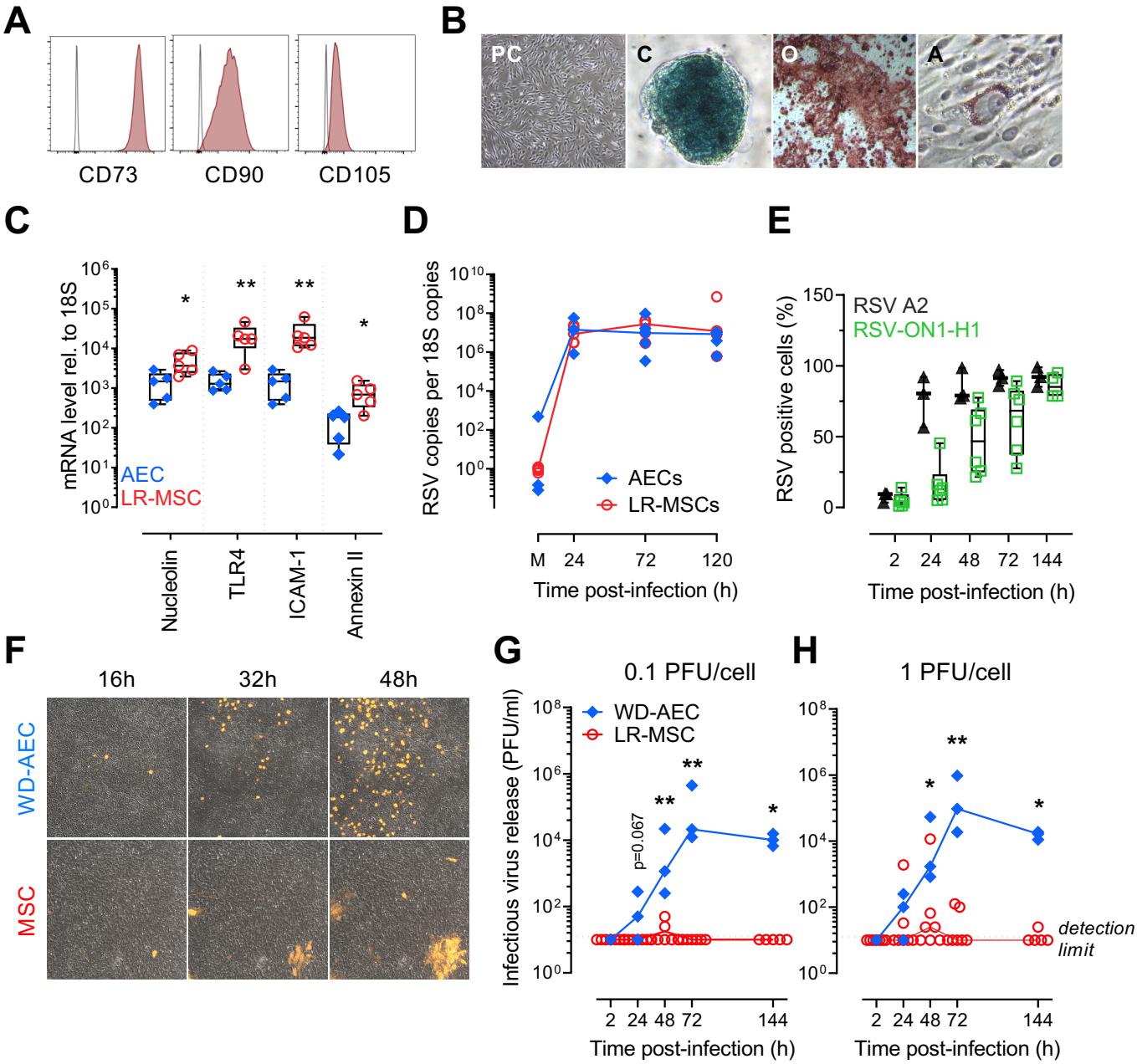
A
CD73
CD90
CD105
B
PC
C
O
A
C
mRNA level rel. to 18S
AEC
LR-MSC
Nucleolin
TLR4
ICAM-1
Annexin II
D
RSV copies per 18S copies
AECs
LR-MSCs
M
24
72
120
Time post-infection (h)
E
RSV positive cells (%)
RSV A2
RSV-ON1-H1
2
24
48
72
144
Time post-infection (h)
F
16h
32h
48h
WD-AEC
MSC
G
0.1 PFU/cell
Infectious virus release (PFU/ml)
WD-AEC
LR-MSC
p=0.067
Time post-infection (h)
H
1 PFU/cell
detection limit
Time post-infection (h)

Fig. 2

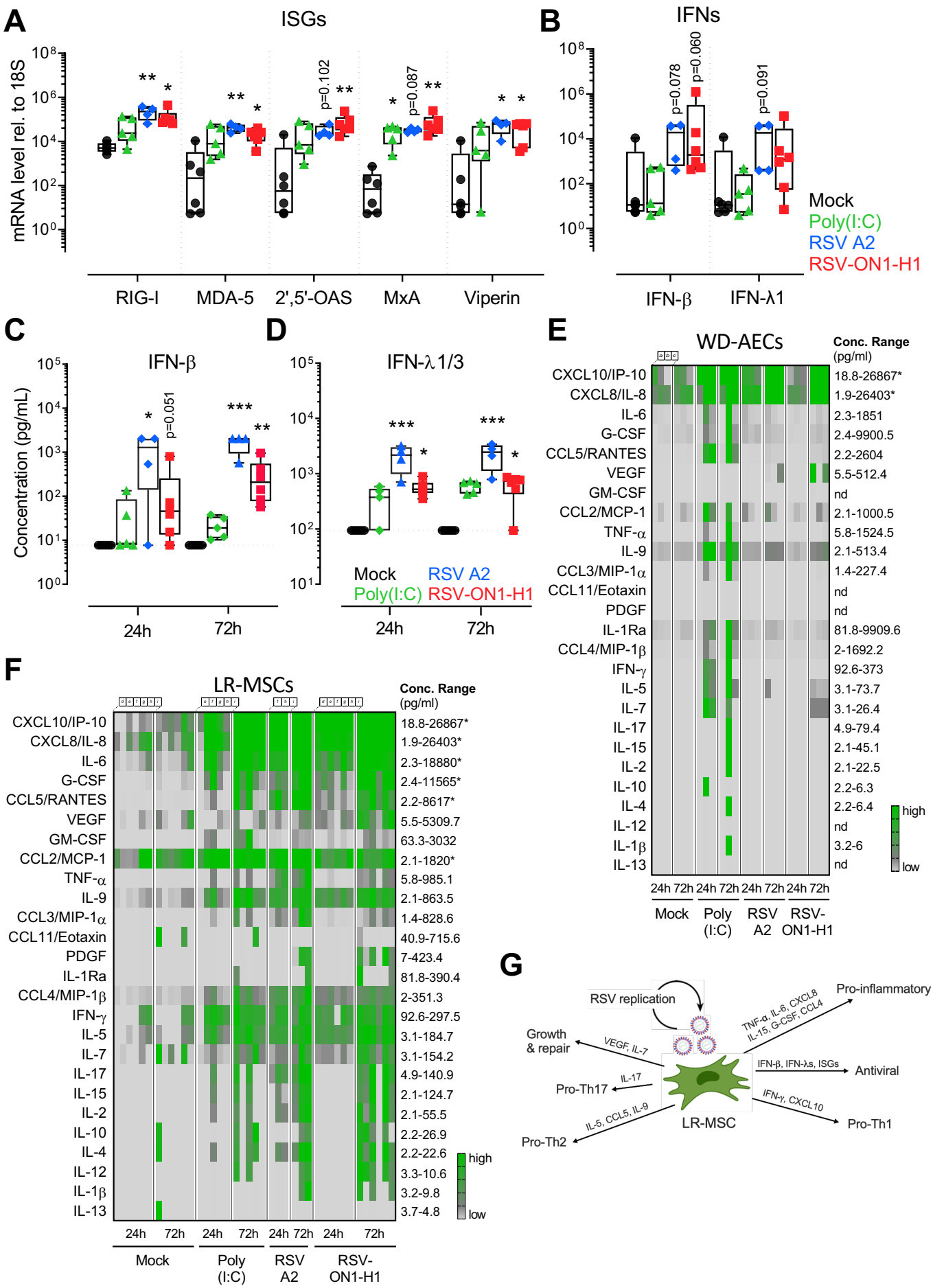
A
ISGs
mRNA level rel. to 18S
RIG-I
MDA-5
2',5'-OAS
MxA
Viperin
p=0.102
p=0.087
B
IFNs
p=0.078
p=0.060
p=0.091
IFN-β
IFN-λ1
Mock
Poly(I:C)
RSV A2
RSV-ON1-H1
C
IFN-β
Concentration (pg/mL)
p=0.051
24h
72h
D
IFN-λ1/3
Mock
RSV A2
Poly(I:C)
RSV-ON1-H1
E
WD-AECs
Conc. Range (pg/ml)
CXCL10/IP-10 18.8-26867*
CXCL8/IL-8 1.9-26403*
IL-6 2.3-1851
G-CSF 2.4-9900.5
CCL5/RANTES 2.2-2604
VEGF 5.5-512.4
GM-CSF nd
CCL2/MCP-1 2.1-1000.5
TNF-α 5.8-1524.5
IL-9 2.1-513.4
CCL3/MIP-1α 1.4-227.4
CCL11/Eotaxin nd
PDGF nd
IL-1Ra 81.8-9909.6
CCL4/MIP-1β 2-1692.2
IFN-γ 92.6-373
IL-5 3.1-73.7
IL-7 3.1-26.4
IL-17 4.9-79.4
IL-15 2.1-45.1
IL-2 2.1-22.5
IL-10 2.2-6.3
IL-4 2.2-6.4
IL-12 nd
IL-1β 3.2-6
IL-13 nd
high
low
Mock
Poly (I:C)
RSV A2
RSV-ON1-H1
F
LR-MSCs
Conc. Range (pg/ml)
CXCL10/IP-10 18.8-26867*
CXCL8/IL-8 1.9-26403*
IL-6 2.3-18880*
G-CSF 2.4-11565*
CCL5/RANTES 2.2-8617*
VEGF 5.5-5309.7
GM-CSF 63.3-3032
CCL2/MCP-1 2.1-1820*
TNF-α 5.8-985.1
IL-9 2.1-863.5
CCL3/MIP-1α 1.4-828.6
CCL11/Eotaxin 40.9-715.6
PDGF 7-423.4
IL-1Ra 81.8-390.4
CCL4/MIP-1β 2-351.3
IFN-γ 92.6-297.5
IL-5 3.1-184.7
IL-7 3.1-154.2
IL-17 4.9-140.9
IL-15 2.1-124.7
IL-2 2.1-55.5
IL-10 2.2-26.9
IL-4 2.2-22.6
IL-12 3.3-10.6
IL-1β 3.2-9.8
IL-13 3.7-4.8
high
low
Mock
Poly (I:C)
RSV A2
RSV-ON1-H1
G
RSV replication
Pro-inflammatory
TNF-α, IL-6, CXCL8
IL-15, G-CSF, CCL4
Growth & repair
VEGF, IL-7
IFN-β, IFN-λs, ISGs
Antiviral
Pro-Th17
IL-17
IFN-γ, CXCL10
Pro-Th1
IL-5, CCL5, IL-9
Pro-Th2
LR-MSC

Fig. 3

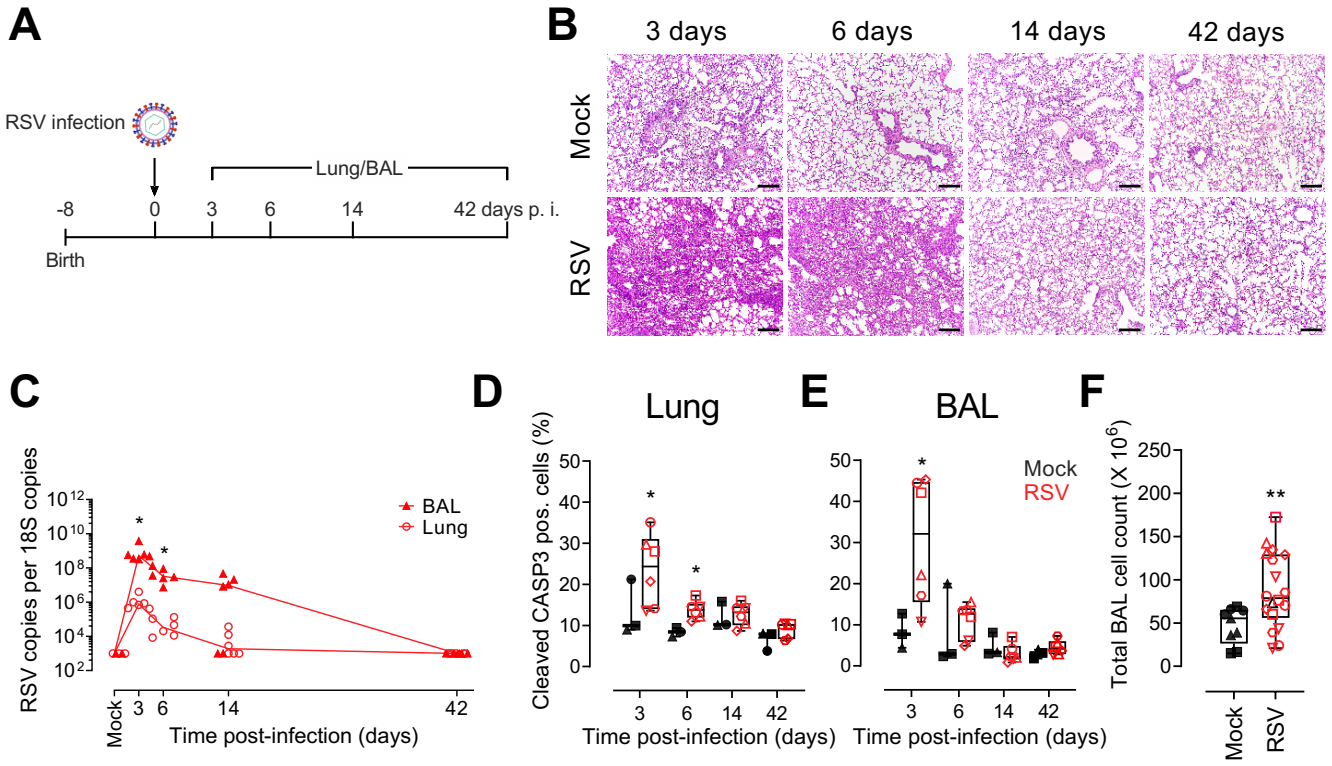
A
RSV infection
Lung/BAL
-8
0
3
6
14
42 days p. i.
Birth
B
3 days
6 days
14 days
42 days
Mock
RSV
C
RSV copies per 18S copies
BAL
Lung
Mock
Time post-infection (days)
D
Lung
Cleaved CASP3 pos. cells (%)
Time post-infection (days)
E
BAL
Mock
RSV
Time post-infection (days)
F
Total BAL cell count (X 10^6)
Mock
RSV

Fig. 4

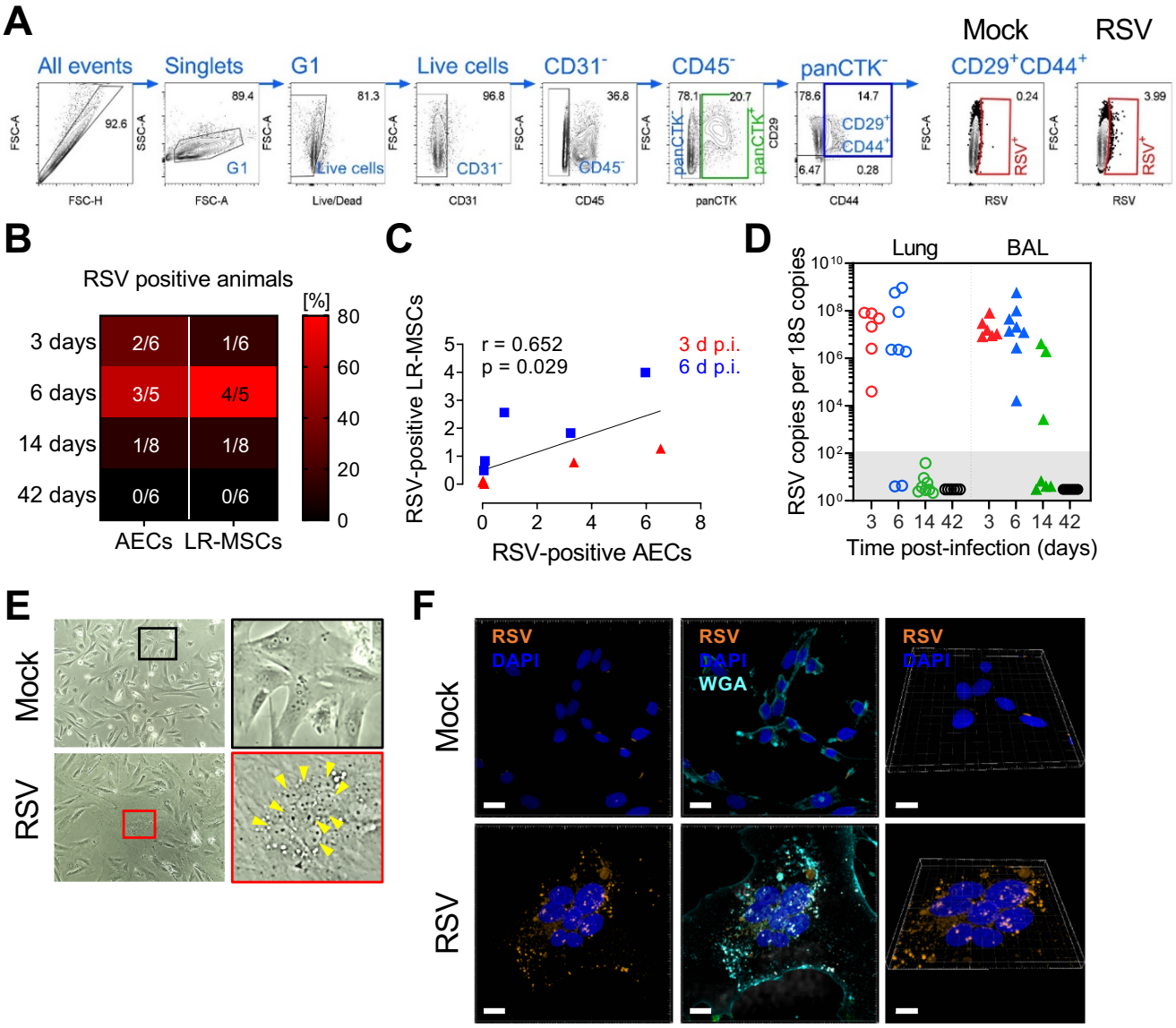
A
All events
Singlets
G1
Live cells
CD31⁻
CD45⁻
panCTK⁻
CD29⁺CD44⁺
Mock
RSV
FSC-H
FSC-A
SSC-A
Live/Dead
CD31
CD45
panCTK
CD29
CD44
RSV
B
RSV positive animals
[%]
3 days
6 days
14 days
42 days
2/6
1/6
3/5
4/5
1/8
1/8
0/6
0/6
AECs
LR-MSCs
C
r = 0.652
p = 0.029
3 d p.i.
6 d p.i.
RSV-positive LR-MSCs
RSV-positive AECs
D
Lung
BAL
RSV copies per 18S copies
Time post-infection (days)
E
Mock
RSV
F
RSV
DAPI
WGA

Fig. 5

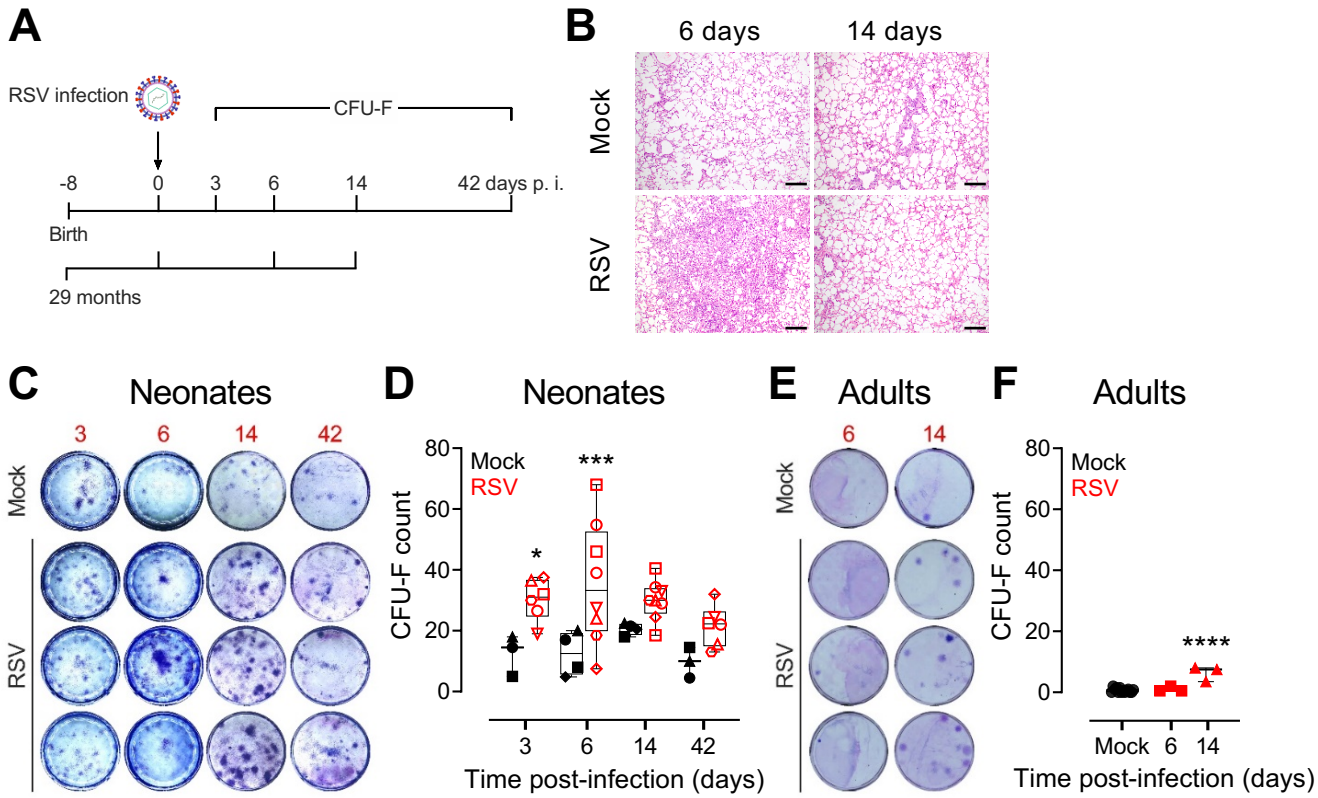
A
RSV infection
CFU-F
-8
0
3
6
14
42 days p. i.
Birth
29 months
B
6 days
14 days
Mock
RSV
C
Neonates
3
6
14
42
Mock
RSV
D
Neonates
CFU-F count
Mock
RSV
*
***
Time post-infection (days)
E
Adults
6
14
Mock
RSV
F
Adults
CFU-F count
Mock
RSV
****
Mock
6
14
Time post-infection (days)

Fig. 6

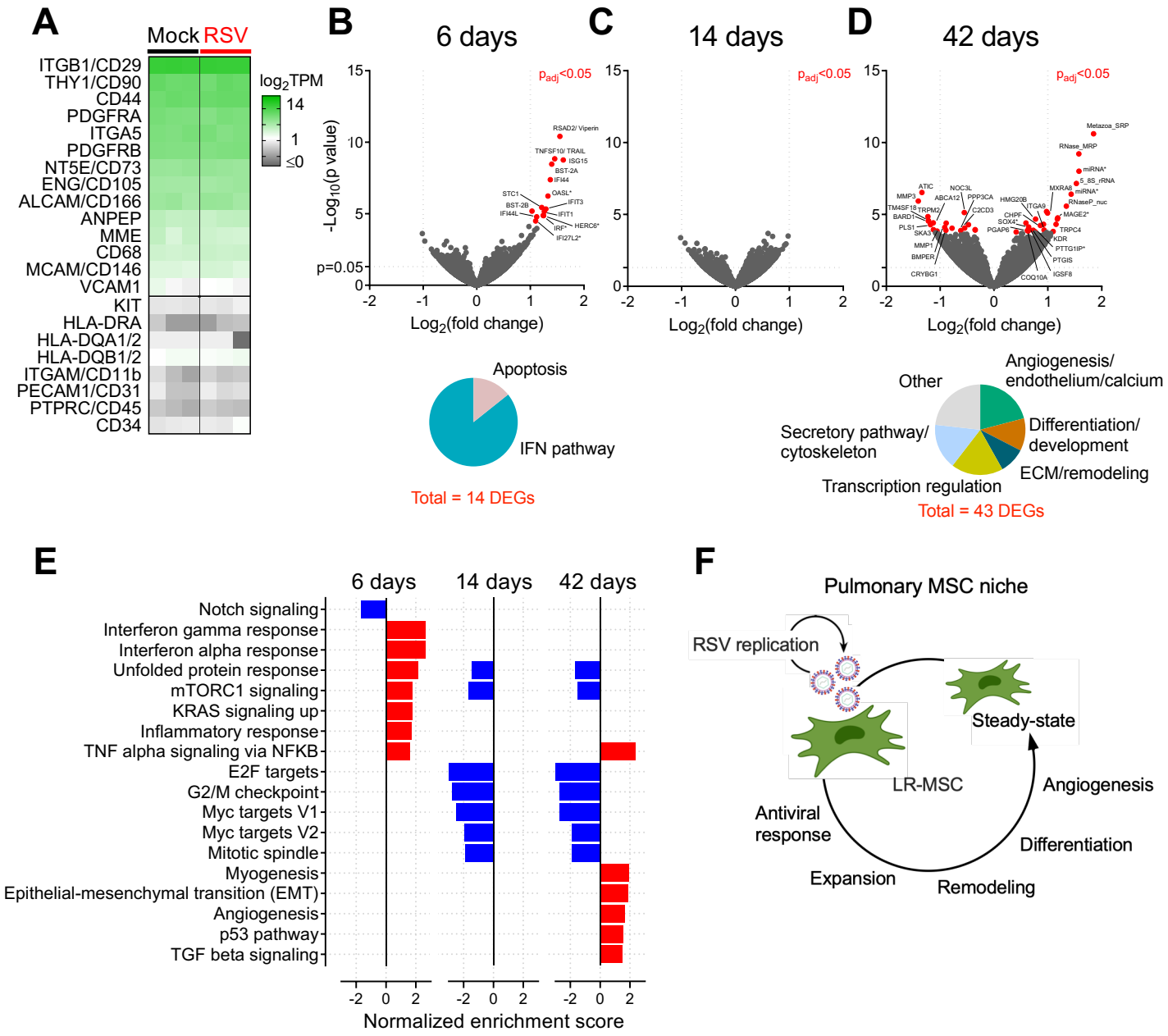
A
Mock RSV
ITGB1/CD29
THY1/CD90
CD44
PDGFRA
ITGA5
PDGFRB
NT5E/CD73
ENG/CD105
ALCAM/CD166
ANPEP
MME
CD68
MCAM/CD146
VCAM1
KIT
HLA-DRA
HLA-DQA1/2
HLA-DQB1/2
ITGAM/CD11b
PECAM1/CD31
PTPRC/CD45
CD34
log2TPM
14
1
≤0
B
6 days
C
14 days
D
42 days
padj<0.05
-Log10(p value)
p=0.05
Log2(fold change)
Apoptosis
IFN pathway
Total = 14 DEGs
Other
Angiogenesis/ endothelium/calcium
Secretory pathway/ cytoskeleton
Differentiation/ development
ECM/remodeling
Transcription regulation
Total = 43 DEGs
E
6 days
14 days
42 days
Notch signaling
Interferon gamma response
Interferon alpha response
Unfolded protein response
mTORC1 signaling
KRAS signaling up
Inflammatory response
TNF alpha signaling via NFKB
E2F targets
G2/M checkpoint
Myc targets V1
Myc targets V2
Mitotic spindle
Myogenesis
Epithelial-mesenchymal transition (EMT)
Angiogenesis
p53 pathway
TGF beta signaling
Normalized enrichment score
F
Pulmonary MSC niche
RSV replication
Steady-state
LR-MSC
Angiogenesis
Antiviral response
Differentiation
Expansion
Remodeling